Nature and Composition of the Lower Continental Crust in Central Spain and the Granulite–Granite Linkage: Inferences from Granulitic Xenoliths

C. VILLASECA[1]*, H. DOWNES[2], C. PIN[3] AND L. BARBERO[4]

[1]DEPARTAMENTO DE PETROLOGÍA Y GEOQUÍMICA, FACULTAD DE CIENCIAS GEOLÓGICAS, UNIVERSIDAD COMPLUTENSE, 28040 MADRID, SPAIN

[2]DEPARTMENT OF GEOLOGY, BIRKBECK COLLEGE, MALET STREET, LONDON WC1E 7HX, UK

[3]CNRS UMR 6524, DÉPARTEMENT DES SCIENCES DE LA TERRE, UNIVERSITÉ BLAISE PASCAL, 5 RUE KESSLER, F-63038 CLERMONT-FERRAND, FRANCE

[4]DEPARTAMENTO DE GEOLOGÍA, FACULTAD DE CIENCIAS DEL MAR, UNIVERSIDAD DE CÁDIZ, 11510 PUERTO REAL (CÁDIZ), SPAIN

*Xenolith-bearing alkaline ultrabasic dykes were intruded into the Hercynian basement of the Spanish Central System in early Mesozoic times. The suite of lower-crustal xenoliths in the dykes can be divided into three groups: felsic peraluminous granulites, metapelitic granulites and charnockitic granulites. The felsic granulites form ~95% of the total volume of the xenoliths, whereas the charnockitic and metapelitic granulites are much less abundant (~0·01 and ~5%, respectively). Thermobarometric calculations based on mineral paragenesis indicate equilibration conditions around 850–950°C, 7–11 kbar; thus the xenoliths represent lower continental crustal material. Superimposed on this high-*T *high-*P *assemblage is a high* T *low* P *paragenesis represented mainly by kelyphitic coronas, reflecting re-equilibration during transport in the alkaline magma. Felsic metaigneous and metapelitic xenoliths exhibit clearly restitic mineral assemblages, with up to 50% garnet and 37% sillimanite. Major and trace element modelling supports the idea that the late Hercynian peraluminous granites of central Spain represent liquids in equilibrium with restitic material of similar composition to the studied lower-crustal xenoliths.* $^{87}Sr/^{86}Sr$ *and* ε_{Nd} *of the felsic xenoliths, calculated at an average Hercynian age of 300 Ma, are in the range 0·706–0·712, and –1·4 to –8·2, respectively. These values match the isotopic composition of the outcropping late Hercynian granites. The Sr isotopic composition of the xenoliths is lower than that of the outcropping mid-crustal lithologies (orthogneisses, pelites). A major contribution from the lower crust to the source of Hercynian granites greatly reduces the necessity of invoking a large mantle contribution in models of granite petrogenesis. The felsic nature of the lower continental crust in central Spain contrasts with the more mafic lower-crustal composition estimated in other European Hercynian areas, suggesting a non-underplated crust in this region of the Hercynian orogenic belt.*

KEY WORDS: *felsic lower continental crust; granulite xenoliths; Sr–Nd isotopes; Hercynian Iberian Belt*

INTRODUCTION

The study of lower-crustal xenoliths has been a powerful tool in understanding the process of anatexis involved in the genesis of felsic magmatism (Downes & Duthou, 1988; Ruiz *et al.*, 1988; Miller *et al.*, 1992; Hanchar *et al.*, 1994; Pankhurst & Rapela, 1995). It is clear that

granite sources in orogenic areas are not the outcropping metamorphic rocks but are located in deeper crustal levels. Lower crust is not easily accessible for study and can also be modified by later orogenic events which could strongly change its primary characteristics (Costa & Rey, 1995). However, in the case of the central Spain, samples of lower-crustal lithologies have been exhumed by anorogenic alkaline magmas. Furthermore, this region has not been affected by metamorphism associated with any orogenic or anorogenic event since the Hercynian orogeny, so the xenoliths are considered to represent the lower crust as it existed at the end of granite emplacement.

The Spanish Central System (SCS) is a major granitoid complex (>10 000 km^2 in surface area) located in the internal part of the Hercynian Iberian Belt (Fig. 1). This huge batholith intruded into continental crust mainly composed of metasedimentary pelitic schists of Precambrian and lower Cambrian age, and metaigneous rocks (orthogneisses) related to early Palaeozoic orogenic events (500 ± 20 Ma, Vialette *et al.*, 1987; Valverde Vaquero *et al.*, 1995). Orthogneisses are the most abundant rocks of the outcropping metamorphic series in the eastern region of the SCS (>80% of surface area in the Guadarrama region; Villaseca *et al.*, 1993). In the western part of the SCS a more complex metasedimentary series is dominant, which is rich in metapsammites with local interlayered carbonate material (Ugidos *et al.*, 1997). During the Hercynian orogeny, this crust evolved from intermediate-P towards low-P, high-T conditions (dated at 335 Ma in the Guadarrama sector; Valverde Vaquero *et al.*, 1995) reaching granulite-facies conditions in wide zones of middle crust with consequent anatexis (e.g. the anatectic granulitic terrane of Toledo; Barbero, 1995).

Granitic plutonism took place in late Hercynian times (325–285 Ma) (Villaseca *et al.*, 1995). The batholith consists mainly of peraluminous granitoids with very scarce basic to intermediate plutonic rocks, and was emplaced at shallow crustal levels [see reviews by Moreno-Ventas *et al.* (1995), Pinarelli & Rottura (1995) and Villaseca *et al.* (1998)]. The lack of appropriate sources in terms of isotopic composition in the vicinity of the Hercynian plutons has led to two models for the origin of the SCS granites: (1) hybridization between crustal melts and mantle-derived magmas (Moreno-Ventas *et al.*, 1995; Pinarelli & Rottura, 1995); (2) partial melting of intracrustal materials (Bea & Moreno-Ventas, 1985; Villaseca *et al.*, 1998). Although the outcropping metaigneous rocks (orthogneisses) more closely approach the isotope signatures of the SCS granites than the metasedimentary rocks, nevertheless they show clear differences in Sr isotope composition compared with the granites (Villaseca *et al.*, 1998). No significant metamorphic event has affected the SCS batholith after its formation; igneous textures are preserved almost without exception.

An alkaline ultrabasic dyke swarm was intruded into the region in early Mesozoic times (Villaseca & Nuez, 1986). These dykes have a N–S orientation and are cut by the tholeiitic Messejana–Plasencia dyke emplaced at ~184 Ma (Schermerhorn *et al.*, 1978). The anorogenic alkaline magmatism is related to North Atlantic rifting during Triassic times (Villaseca *et al.*, 1992). The dykes, which are mainly ultrabasic camptonitic lamprophyres, contain a varied population of mainly felsic granulitic xenoliths (Villaseca & Nuez, 1986). These granulite xenoliths show very distinctive petrographic, mineralogical and geochemical characteristics compared with the outcropping Hercynian granulitic terranes in central Spain.

In this paper we present a petrographic, mineralogical, geochemical and isotopic (Sr, Nd) study of the granulitic xenolith suite from the SCS that indicates a felsic restitic character for the lower continental crust in this region. The role played by the late Hercynian granitic magmatism in the generation of this restitic lower crust, and the differences between granulitic material at lower- and middle-crustal levels (xenoliths and outcropping granulitic terranes, respectively), are also discussed.

PREVIOUS ESTIMATES OF LOWER-CRUSTAL COMPOSITION IN CENTRAL SPAIN: GEOPHYSICAL DATA

Deep seismic profiles constrain the general crustal structure of central Spain. Banda *et al.* (1981) showed that the crust in this area is around 31 km thick and consists of four layers (Fig. 2):

(1) a sedimentary cover up to 3 km thick, with P-wave velocities <3·5 km/s;

(2) an upper crystalline layer up to 11 km thick, including a low-velocity layer extending from about 7 to 11 km (V_p = 5·6 km/s), with P-wave velocities in the range 5·6–6·1 km/s;

(3) middle crust from 11 to 23 km depth and V_p ~ 6·4 km/s;

(4) lower crust from 23 to 31 km depth and V_p = 6·8–6·9 km/s.

Gravity and magnetotelluric data from Carbó & Capote (1985) corroborate the described stratigraphy of the crust in central Spain. More recently, deep seismic sounding undertaken by the Iberian Lithosphere Heterogeneity and Anisotropy Project showed the continental crust of the SCS to be 34 km thick, with the upper boundary of the lower crust located between 21 and 23 km depth (ILIHA DSS Group, 1993). The boundary between middle and lower crust is always well marked by an increase in P-wave velocity up to 6·7–6·8 km/s.

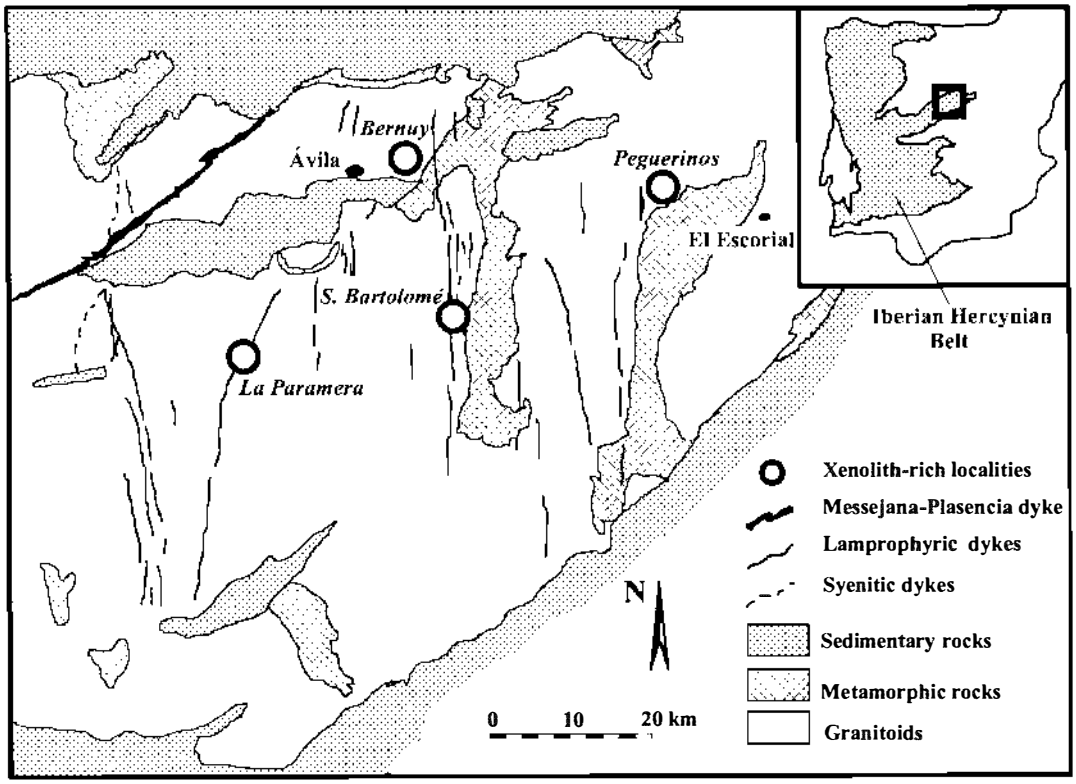

Fig. 1. Geological map of central Spain showing lamprophyric dykes and the location of the main outcrops with granulitic xenoliths.

However, models derived from ILIHA crustal data show that there are no significant lateral inhomogeneities in gross crustal structure, in marked contrast to the heterogeneous Hercynian surface geology.

Data from P-wave coda in the SCS (Paulssen & Visser, 1993) also confirm a continental crust of around 30 km in thickness, similar to the average crustal thickness of Phanerozoic fold belts of central Europe (Wedepohl, 1995). The lowermost 8 km correspond to the granulitic lower crust with P-wave velocities always in the range of 6·5–6·9 km/s. These values are more typical of felsic or pelitic compositions rather than mafic granulites (V_p from 6·9 to 7·5 km/s; Rudnick, 1992; Wedepohl, 1995). P-wave velocities in the range 6·8–7·0 km/s are very common in garnet-bearing peraluminous granulites (Kern, 1990), these being one of the most abundant lithologies in the xenolith suite of the SCS (Villaseca & Nuez, 1986). In Fig. 2, a sketch profile of the SCS crust is compared with the average continental crust of Wedepohl (1995).

From seismological data there does not seem to be a significant mafic granulitic or eclogitic layer in the lower crust of the SCS, which agrees with the lithologies of the granulitic xenoliths studied in this work. Wedepohl (1995) stated that in the younger fold belts in Central Europe, mafic granulites occur locally as voluminous bodies but more commonly as a thin layer above the Moho. Also, some recent xenolith studies (e.g. Hanchar *et al.*, 1994) indicate that the lower continental crust may contain a larger supracrustal component than previously thought. Thus, in some regions, the lower-crustal composition may be closer to tonalite rather than diorite as previously estimated (Wedepohl, 1995). McLennan & Taylor (1996) also recognized that estimates of the average composition of the continental crust may be shifted towards a more acid composition.

TYPES OF GRANULITIC XENOLITHS

Although granulitic xenoliths occur in camptonitic dykes in several places in the SCS, two localities are most important because of the large number and variety of xenoliths found in them. The first is a diatreme-like outcrop in La Paramera (Nuez *et al.*, 1981). It is composed of breccia, and has a surface area of around 20 000 m^2. The outcrop is elliptical in shape, with its long axis striking N–S, the same direction as the dykes. In this locality, 25% of the breccia is composed of granitic and other wall-rock xenoliths and xenocrysts, as well as granulite xenoliths. The second important locality is the dyke swarm of Peguerinos (Fig. 1) where the narrow

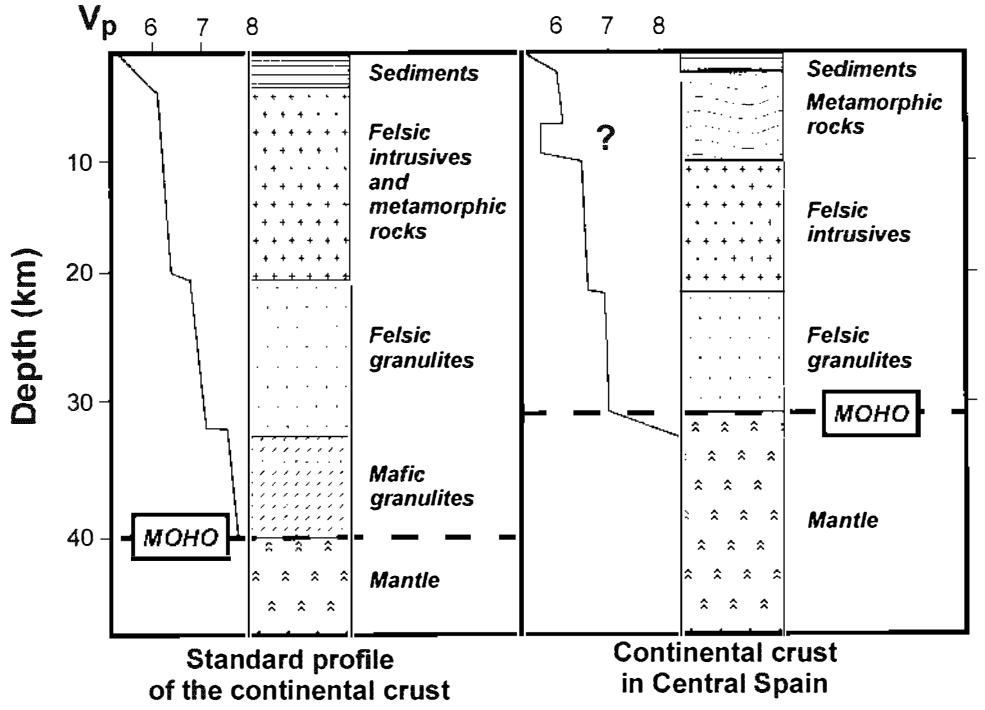

Fig. 2. Standard profile of the continental crust from Wedepohl (1995) compared with the estimated continental crust in central Spain. Data from Wedepohl are derived from integrated 3000 km long European Geotraverse data from central Spain on the basis of geophysical and petrological arguments. V_p values are in km/s. (See text for further explanation.)

(<0·5 m wide) lamprophyric dykes carry 10–20 vol. % of granulitic xenoliths. Xenoliths were also found in dykes at Bernuy and San Bartolomé (Fig. 1).

Several kinds of xenoliths are found. The largest (up to 1 m^3) and more angular types are granitic rock fragments, similar to the country rocks, and varied metamorphic country rock enclaves. However, the most abundant xenoliths are granulites with a characteristic rounded shape as a consequence of longer transport in the dyke. They can reach up to 10 000 cm^3 in volume (Table 1), which implies high emplacement velocities of the host magma, to inhibit settling of the xenoliths (velocities of the order of 10–100 m/h can be deduced from Stokes' law). This rapid ascent of the xenoliths inhibits the development of significant contact metamorphism, even in the smallest samples, which are a few millimetres in diameter. Nevertheless, local intergranular recrystallization processes and development of kelyphitic coronas around garnet are commonly observed.

More than 70 granulite xenoliths have been collected for this study. We sampled four main outcrops which contain abundant xenoliths (Fig. 1), covering an area of the SCS of >1000 km^2. Three main types can be distinguished (Table 1):

Type 1: charnockitic granulites. These are small pyroxene-bearing xenoliths, without peraluminous minerals such as garnet, phlogopite or sillimanite. They vary from felsic (sample U-3: a charnockite with plg + qtz + kfs + opx) towards intermediate types (sample U-28: a metanorite with plg + opx + cpx). Charnockitic granulite xenoliths are very scarce and have been found only in two localities. They show typical fine-grained granoblastic textures (see Appendix A).

Type 2: felsic peraluminous granulites. This group includes quartzo-feldspathic garnet-bearing types of which two subtypes have been identified: (2a) granulites with accessory orthopyroxene (kfs + plg + qtz + grt + opx ± phl); (2b) granulites without orthopyroxene, and with accessory phlogopite, aluminium silicate or both (Table 1). Type 2b is the most abundant of all the granulitic xenoliths of the SCS.

Type 3: pelitic peraluminous granulites. These are granulites with parageneses similar to that of the 2b type but with >30% of peraluminous minerals (garnet, aluminium silicate); usually sillimanite forms >8% in volume. The most common paragenesis is grt + kfs + plg + qtz + sill. A subtype (3b) can be distinguished as highly garnet–sillimanite-rich xenoliths, with accessory amounts of quartz and feldspars (sample U-10, Table 1).

These two latter types appear in two textural varieties: (a) foliated or banded granoblastic types, with segregated

Table 1: Mineral assemblages of the granulite xenoliths

	Charnockites		Felsic meta-igneous											Metapelites						
Xenolith type:	1	1	2a	2a	2b	2b	2b	2b	2b	2b	2b	2b	2b	3a	3a	3a	3a	3a	3b	3b
Sample no:			U-141	U-140			U-93	U-157	U-153	U-156	U-92	U-145	U-152	U-96	U-90	U-91			AR-153	
	U-3	U-28	81846	81845	U-49	U-50	77748	95153	95149	95152	77747	95141	95148	77750	77745	77746	U-42	U-46	81938	U-10
Quartz	17		18	3	30	3	42	33	22	17	25	24	12	18	1	15	13	15	10	
K-feldspar	17		20	47	43	32	35	11	25	31	46	55	68	45	16	39	33	40	19	
Plagioclase	54	64	46	32	10	19	27	39	29	30			3		29	10	10			2
Garnet/																				
(kelyph)*			12	10	14	(40)	(3)	15	(18)	(20)	21	17	15	22	(38)	(26)	(28)	(30)	(40)	(52)
Phlogopite			1		1	1		2	2				tr.							
Sillimanite										1	7	3	2	13	11	8	14	12	27	37
Ortho-																				
pyroxene	10	29	2	5																
Clino-																				
pyroxene		5																		
Rutile		1		1	1	1		tr.	tr.	1	1	1		1	2	1	1	2	3	2
Apatite	1				tr.															
Zircon/																				
monazite			tr.		tr.	tr.	tr.					tr.	tr.	tr.			tr.	tr.	tr.	
Opaques	1	1	1	1	tr.	tr.	1	1	1	tr.	tr.	tr.	1	tr.	2	1	1	1	1	1
Vol. xeno-																				
lith (cm^3)	1·6	0·5	25	3	700	1000	450	1080	180	2200	?	900	1450	700	250	110	62	125	1	130
Size (cm)	2 × 0·8	1 × 0·5	3·5 × 2·5	3 × 1	7 × 10	10 × 10	8 × 7 × 8	9 × 10 × 12	6 × 6 × ?	15 × 12	?	12 × 8	13 × 10	7 × 10	6 × 7 × 6	5 × 5·5 × 4	5·5 × 3·2	5·5 × 4·5	1 × 1	5·7 × 4·5
Estimated																				
density																				
(g/cm^3)	2·72	2·98	2·80	2·75		3·05	2·89		2·80			2·88	2·86	2·93	3·14		3·11			3·66

*When garnet is substantially substituted by kelyphitic coronas (>50% in surface area) their relative modal proportion is given in parentheses. Minerals forming kelyphitic coronas (orthopyroxene, spinel, feldspars, etc.) are not distinguished in this table. Density estimations are made on the basis of estimated mineral mode. (See text for further explanation.)

garnet-rich bands and narrow leucocratic veins in some samples; (b) massive granoblastic types with a weak mineral orientation. Further petrographical information is included in Appendix A.

The relative proportions of the three types of xenoliths are 5:68:27. If instead of considering the number of xenoliths we consider their relative volume (see Table 1), as type 1 xenoliths are always very small and scarce, the volume abundance would be around 0·01:95:5. We consider these relative proportions to be representative of the SCS lower crust as, from the estimated densities of the xenoliths (Table 1), no preferential removal by settling would be expected. Thus, felsic peraluminous granulites form almost the entire granulitic xenolith suite, with the pelitic and charnockitic types being very scarce.

ANALYTICAL METHODS

Mineral compositions were determined by electron microprobe at the Complutense University of Madrid (Jeol Superprobe JXA 8900-M) and St Andrews University (UK) (Jeol Superprobe 733). In both cases, operating conditions were 15 kV, 20 nA and a beam diameter of 2–5 μm, and the ZAF correction procedure was used.

Major and trace element analyses of six samples were determined at the CNRS CRPG Nancy by inductively coupled plasma atomic emission spectrometry (ICP-AES) for major elements and ICP mass spectrometry (ICP-MS) for trace elements. Six samples from Villaseca & Nuez (1986) are also included; rare earth element (REE) data for two of them were determined at the CNRS–CRPG Nancy by ICP-AES following the method of Govindaraju & Mévelle (1987). Another group of six samples was analysed for major and trace elements by XRF, except for REE which were measured by ICP-AES, at Royal Holloway, University of London.

Sixteen xenoliths were selected for isotopic analysis. Six Sr and Nd isotopic determinations were performed at the CNRS–UMR 6524 (Clermont-Ferrand) using an automated VG 54E double collector thermal ionization mass spectrometer. Sm and Nd contents were measured by isotope dilution mass spectrometry at CNRS–UMR 6524. Analytical procedures for the isotopic data at this laboratory have been described by Pin *et al.* (1990). Another six samples were analysed at Royal Holloway, University of London, using an automated VG 354 multicollector thermal ionization mass spectrometer. Analytical procedures for Royal Holloway isotopic data have been described by Downes *et al.* (1997). A further four samples for Sr and Nd isotopic determinations were analysed at the CAI de Geocronología y Geoquímica Isotópica of the Complutense University of Madrid, using an automated VG Sector 54 multicollector thermal ionization mass spectrometer with data acquired in multi-dynamic mode. Analytical procedures for the isotopic data at this laboratory have been described by Reyes *et al.* (1997). Repeated analysis of NIST SRM 987 Sr standard gives $^{87}Sr/^{86}Sr = 0{\cdot}710209 \pm 9$ (2σ, $n = 10$) (Clermont-Ferrand), $0{\cdot}710252 \pm 21$ (2σ, $n = 31$) (London) and $0{\cdot}710256 \pm 8$ (2σ, $n = 27$) (Madrid). During the course of this study the La Jolla Nd standard gave $^{143}Nd/^{144}Nd = 0{\cdot}511858 \pm 7$ (2σ, $n = 4$) (Clermont-Ferrand). In London, an internal (Aldrich) Nd standard gave a $^{143}Nd/^{144}Nd$ value of $0{\cdot}511418 \pm 6$ (2σ, $n = 21$) equivalent to a La Jolla value of 0·511856. In the Madrid laboratory the Nd standard used was JM and the result obtained was $0{\cdot}511810 \pm 4$ ($n = 16$). This latter value is similar to that obtained by Moreno-Ventas *et al.* (1995) (0·511821) for an aliquot of the same Nd standard. These standard results indicate similar reproducibility in the three laboratories. ε_{Nd} values were calculated using the following bulk Earth parameters: $^{143}Nd/^{144}Nd = 0{\cdot}512638$; $^{147}Sm/^{144}Nd = 0{\cdot}1967$. The 2 SD error on ε_{Nd} calculations is $\pm 0{\cdot}4$.

PETROGRAPHY AND MINERAL CHEMISTRY

K-feldspar

K-feldspar is usually the most abundant felsic mineral in both felsic and pelitic xenoliths (Table 1). They show high Na_2O and CaO contents (up to 3·5 wt % Na_2O and 1·5 wt % CaO, see Table 2). P_2O_5 contents are in the range of 0·17–0·30 wt %. These values are higher than those typical of K-feldspar from Hercynian granites of the area (0·03–0·15 wt %; López Moro *et al.*, 1997) and are more typical of feldspars from P-rich granites (Breiter, 1998; Sha & Chappell, 1998). In small xenoliths or in the rims of large xenoliths, micropegmatitic and symplectitic intergrowths between K-feldspar and plagioclase appear, indicating local recrystallization of feldspars.

Plagioclase

Plagioclase is present in most of the peraluminous xenoliths and also in the scarce mafic meta-noritic types of the charnockitic suite. Its composition varies depending on the xenolith type. In the meta-noritic xenoliths it is andesine (An_{45}) with around 1·0 wt % K_2O (Fig. 3); in the felsic peraluminous xenoliths its composition varies between An_{21} and An_{35} with 1·7–3·7 wt % K_2O (Fig. 3). This corresponds to 10–23% of molecular orthoclase component and is 5–7 times higher than that of the plagioclase from pelitic and felsic granulites from middle-crustal levels of the area (Barbero, 1995). P_2O_5 contents are in the range of 0·14–0·23 wt %, suggesting that both

Table 2: Representative electron microprobe analyses (I)

	K-feldspar				
Xenolith type:	2a	2b	2b	3	3
Sample:	81846	95148	99193	77750	U-46
Analysis no.:	6	26	36	2	13
	Kelyph				
SiO_2	60·77	63·42	63·64	61·99	63·50
TiO_2	0·06	0·03	0·00	0·07	0·10
Al_2O_3	19·43	19·69	18·73	21·07	19·00
FeO	1·30	0·01	0·03	0·06	0·08
MnO	0·02	0·01	0·00	0·08	0·04
MgO	0·46	0·01	0·00	0·01	0·01
CaO	1·24	1·48	0·03	0·64	0·78
Na_2O	0·10	3·56	0·44	3·08	0·77
K_2O	14·60	10·59	15·53	10·47	13·73
Total	97·99	98·81	98·40	97·49	98·23
Cations on the basis of 32 oxygens					
Si	11·539	11·695	11·924	11·545	11·869
Ti	0·009	0·004	—	0·010	0·014
Al	4·345	4·277	4·132	4·620	4·186
Fe	0·206	0·001	0·005	0·009	0·013
Mn	0·004	0·002	—	0·013	0·006
Mg	0·131	0·002	—	0·003	0·003
Ca	0·252	0·293	0·007	0·128	0·156
Na	0·038	1·274	0·159	1·112	0·279
K	3·536	2·492	3·712	2·488	3·274
End-members					
Ab	1·0	31·4	4·1	29·8	7·5
Or	92·4	61·4	95·7	66·7	88·3
An	6·6	7·2	0·2	3·4	4·2

feldspars are major P carriers in these xenoliths. The rims of the plagioclase crystals show frequent microgranophyric or microsymplectitic aggregates, which are interpreted to result from intergranular recrystallization during transport in the alkaline magma. In these symplectitic rims the composition of the plagioclase becomes more calcic (An_{30} to An_{42}, sample 81846, Table 2) and poorer in orthoclase (Or_{64} to Or_{24}, sample 81846, Table 2), thus approaching the typical plagioclase composition of kelyphitic coronas (Fig. 3).

Garnet

With the exception of the charnockitic xenoliths, garnet is present in the entire suite. Its modal proportion varies from 10 to 25% in the felsic types, and from 25 to 52% in the pelitic xenoliths (Table 1). Garnet frequently contains inclusions of quartz, phlogopite, rutile, zircon, sillimanite, plagioclase and pyrrhotite. In some samples acicular sillimanite inclusions define a relict foliation in the garnet. Garnets are variably transformed to dark kelyphitic coronas, which in some cases completely pseudomorph the original crystal.

The garnet belongs to the almandine–pyrope series, and has a relatively constant composition. Grossular is always <5·5% mol and spessartine <2 mol % (Table 2). Garnets in pelitic xenoliths are slightly richer in Fe than those in felsic types (Fig. 4). When compared with garnets of the outcropping granulitic terranes of the area, those of the xenoliths are richer in pyrope (35–55 mol %), which reflects greater depths of equilibration (Fig. 4). Compositional zoning is almost absent in the garnet core, but there is a notable decrease in Ca towards a narrow rim (Fig. 4), with a subtle increase in the Fe/Mg ratio (Table 2). This is interpreted as a consequence of decompression during transport to the surface.

Pyroxenes

In the charnockitic xenoliths orthopyroxene occurs in textural equilibrium with augitic clinopyroxene. This orthopyroxene is En_{63} in composition (Table 2) and shows a slight increase in MgO/(MgO + FeO) ratio from core to rim. The augitic clinopyroxene is relatively rich in Al_2O_3 (up to 2·5 wt %) and contains up to 0·5 wt % Na_2O (Table 2). Orthopyroxene also occurs as an accessory phase in textural equilibrium with garnet in some felsic xenoliths (type 2a), where it is enstatitic in composition (around En_{60}–En_{65}) and rich in Al_2O_3 (up to 7 wt %, sample 81846, Table 2). No systematic core–rim compositional variations have been found.

Phlogopite

Mica is present only in the felsic peraluminous xenoliths. In contrast to the outcropping granulitic terranes, mica in the granulitic xenoliths is a phlogopite (Table 2). It is rich in TiO_2 (5·6 wt %), typical of high-temperature micas, and F (up to 2·5 wt %), and must be H_2O poor (Fig. 5). The low Al_2O_3 contents of these phlogopites (~15 wt %), compared with biotites of the middle-crustal granulites of the Anatectic Complex of Toledo (Fig. 5), is typical of phlogopites that are residual after high-temperature dehydration-melting reactions (Singh & Johannes, 1996).

Sillimanite

In peraluminous xenoliths prismatic sillimanite is present in variable amounts (Table 1). It is a major mineral in

Table 2: Representative electron microprobe analyses (1)

	Plagioclase										
Xenolith type:	1	2a	2a	2a	2b	2b	2b	2b	2b	2b	2b
Sample:	U-28	81845	81846	81846	95151	95151	95151	99193	99185	95148	81841
Analysis no.:	24	119	35 core	34 sym rim	17	160 sym rim	1 kelyph	37	3	25	4
SiO_2	56·19	60·06	62·43	58·21	59·11	61·13	50·95	60·15	60·98	59·61	59·04
TiO_2	0·02	0·00	0·00	0·08	0·12	0·07	0·08	0·05	0·09	0·07	0·02
Al_2O_3	26·91	24·39	23·46	26·49	25·56	22·58	30·99	24·20	23·13	24·25	25·37
FeO	0·15	0·02	0·08	0·29	0·80	0·17	0·38	0·08	0·09	0·12	0·11
MnO	0·02	0·00	0·04	0·01	0·00	0·00	0·02	0·01	0·01	0·00	0·00
MgO	0·04	0·00	0·01	0·08	0·13	0·00	0·00	0·01	0·01	0·02	0·00
CaO	8·88	6·39	5·73	8·51	4·03	6·17	13·61	6·07	4·76	6·58	7·04
Na_2O	5·83	6·23	7·06	6·26	5·92	6·28	2·91	6·75	5·93	6·03	6·79
K_2O	1·15	2·04	1·07	0·44	3·73	1·38	0·32	2·13	3·90	2·51	0·99
Total	99·18	99·12	99·87	100·35	99·39	97·77	99·27	99·44	98·89	99·18	99·35
Cations on the basis of 32 oxygens											
Si	10·212	10·831	11·092	10·395	10·693	11·114	9·329	10·834	11·061	10·787	10·625
Ti	0·003	—	—	0·010	0·017	0·010	0·011	0·007	0·012	0·009	0·002
Al	5·758	5·179	4·908	5·570	5·445	4·835	6·683	5·133	4·940	5·169	5·377
Fe	0·022	0·003	0·012	0·043	0·121	0·025	0·058	0·012	0·013	0·018	0·017
Mn	0·002	—	0·005	0·001	—	—	0·004	0·002	0·002	—	—
Mg	0·010	—	0·003	0·021	0·036	—	—	0·003	0·002	0·005	—
Ca	1·730	1·234	1·090	1·628	0·781	1·201	2·670	1·172	0·924	1·276	1·357
Na	2·053	2·179	2·432	2·166	2·077	2·213	1·032	2·356	2·086	2·115	2·370
K	0·267	0·469	0·241	0·100	0·860	0·319	0·076	0·489	0·902	0·579	0·226
End-members											
Ab	50·7	56·1	64·6	55·6	55·9	59·3	27·3	58·7	53·3	53·3	60·0
Or	6·6	12·1	6·4	2·6	23·1	8·5	2·0	12·2	23·1	14·6	5·7
An	42·7	31·8	29·0	41·8	21·0	32·2	70·7	29·2	23·6	32·1	34·3

pelitic xenoliths. Sillimanite contains appreciable FeO and MgO (0·74 wt % and 0·18 wt %, respectively) (Table 2). In some xenoliths, small green spinel crystals surround the aluminium silicate, which is a typical decompressional feature related to magmatic transport of the xenolith.

Accessory minerals

Common accessory phases in the felsic peraluminous and pelitic xenoliths are rutile and, in lesser amounts, ilmenite. Rutile is conspicuous in all the xenoliths, appearing as euhedral crystals typically 100–250 μm in size. They can contain ~0·4 wt % FeO (Table 2). Ilmenite is Mn rich with up to 4·5 wt % MnO. Other accessory phases include acicular graphite, usually found as inclusions in the aluminium silicates of pelitic xenoliths, pyrrhotite, pyrite and chalcopyrite. Scanning electron microscopy (SEM) studies reveal that zircon and monazite are also present but in trace amounts, much less abundant than in the granulites of mid-crustal terranes. Zircons are typically rounded (35–65 μm) with corroded cores showing zoning patterns truncated by outer unzoned rims. These zircons are very similar to type-B of Watt *et al.* (1996). Monazites are rounded subhedral crystals (35–120 μm) and usually unzoned. Apatite is very rare, being more abundant in the charnockitic varieties (Table 1).

Kelyphitic coronas

Kelyphitic coronas around garnet are formed of a microcrystalline symplectitic aggregate of spinel,

Table 2: Representative electron microprobe analyses (III)

	Garnet										
Xenolith type:	2a	2a	2a	2b	2b	2b	2b	2b	3	3	3
Sample:	81845	81845	81846	99185	99185	99151	95151	95148	77750	77750	U-46
Analysis no.:	137	131	40	14	4	168	171	18	8	15	11
	core	rim		core	rim	core	rim		core	rim	
SiO_2	40·08	34·55	40·28	39·59	39·82	40·47	40·52	39·33	38·52	39·38	39·54
TiO_2	0·16	0·13	0·05	0·18	0·10	0·13	0·06	0·08	0·14	0·08	0·13
Al_2O_3	22·51	23·35	22·54	22·48	22·97	22·72	23·13	23·41	22·04	21·93	22·08
Cr_2O_3	n.d.	n.d.	0·04	0·04	0·02	n.d.	n.d.	n.d.	0·01	0·00	0·05
FeO	24·66	28·57	24·00	23·52	24·10	23·21	24·69	20·61	28·16	27·02	26·58
MnO	0·34	0·45	0·54	0·46	0·49	0·28	0·27	0·24	0·36	0·37	0·30
MgO	11·37	12·12	11·67	11·74	11·85	13·02	13·18	14·80	9·13	9·41	9·10
CaO	1·47	0·39	0·96	1·65	1·04	1·03	0·20	0·80	1·06	1·33	1·90
Na_2O	0·00	0·00	0·03	0·02	0·02	0·00	0·00	0·00	0·00	0·00	0·00
Total	100·58	99·56	100·19	99·68	100·40	100·86	102·04	99·27	99·43	99·52	99·68
Cations on the basis of 24 oxygens											
Si	6·043	5·269	6·085	5·999	5·991	6·024	5·973	5·863	5·972	6·080	6·065
Ti	0·018	0·015	0·006	0·021	0·011	0·014	0·006	0·009	0·016	0·010	0·015
Al	3·996	4·195	4·010	4·010	4·070	3·984	4·015	4·111	4·025	3·988	3·992
Cr	—	—	0·004	0·004	0·002	—	—	—	0·001	—	0·006
Fe	3·109	3·644	3·032	2·981	3·033	2·890	3·043	2·570	3·652	3·488	3·410
Mn	0·043	0·057	0·069	0·060	0·062	0·036	0·034	0·030	0·047	0·048	0·039
Mg	2·554	2·756	2·628	2·651	2·657	2·888	2·897	3·288	2·110	2·167	2·081
Ca	0·238	0·064	0·156	0·268	0·167	0·164	0·032	0·128	0·176	0·219	0·312
Na	—	—	0·009	0·005	0·007	—	—	0·001	0·001	—	—
End-members											
Alm	52·30	55·88	51·44	49·98	51·18	48·34	50·67	42·71	61·00	58·90	58·37
Grs	4·00	0·99	2·53	4·39	2·76	2·74	0·53	2·13	2·91	3·70	5·34
Prp	42·98	42·26	44·59	44·45	44·84	48·32	48·23	54·65	35·25	36·58	35·62
Sps	0·72	0·88	1·17	1·00	1·04	0·61	0·56	0·51	0·78	0·82	0·67

orthopyroxene, feldspars and scarce quartz. In some xenoliths, development of the kelyphitic coronas around garnet replaces most of the garnet crystal. The coronas usually thicken towards the border of the xenolith, the outermost garnets being totally pseudomorphed by the kelyphitic aggregate. Spinel is usually found in these coronas, but is absent in the matrix. Its composition is intermediate between hercynite and spinel (around 60 wt % hercynite). Zn is very low (<0·8 wt %, Table 2) as expected in low-pressure recrystallization (Nichols *et al.*, 1992). Zoning is apparent in the spinel, with the amount of hercynite increasing towards the rim (see sample 99193 in Table 2).

Kelyphitic orthopyroxenes have a variable composition between En_{50} and En_{55} (Table 2). Their Fe/Mg ratio is higher than that of the matrix orthopyroxene in the felsic peraluminous xenoliths (type 2a). The coronitic orthopyroxenes also have lower Ti (in type 2a xenoliths), Mg and Cr contents, and higher Al_2O_3 (up to 13 wt %), Ca and Mn (up to 0·7 wt %) contents.

Plagioclase microcrystals associated with the kelyphitic coronas have a highly calcic (up to An_{71}) composition compared with the matrix plagioclase (Fig. 3) and a lower orthoclase content (Fig. 3). K-feldspar in the kelyphitic coronas is richer in FeO than other sanidines in these xenoliths (Table 2). These alkali feldspars with a more

Table 2: Representative electron microprobe analyses (IV)

	Orthopyroxene								Clinopyroxene	
Xenolith type:	1	2a	2a	2a	2b	2b	3	3	1	1
Sample:	U-28	81845	81846	81846	95151	99193	77750	U-46	U-28	U-28
Analysis no.:	1	121	19	26 Kelyph	12 Kelyph	15 Kelyph	16 Kelyph	25 Kelyph	15	16
SiO_2	52·20	49·90	50·45	45·53	44·85	44·80	43·23	44·00	51·57	51·65
TiO_2	0·19	0·27	0·23	0·08	0·28	0·90	0·03	0·13	0·49	0·46
Al_2O_3	1·45	5·51	7·16	11·39	13·80	12·25	13·68	14·40	2·50	2·48
FeO	19·52	22·74	20·56	25·82	22·40	22·27	25·56	25·30	8·19	8·23
MnO	0·31	0·09	0·17	0·69	0·28	0·34	0·42	0·23	0·16	0·14
MgO	24·94	20·65	21·14	16·10	18·16	17·93	15·23	15·09	14·74	17·77
CaO	1·13	0·23	0·13	0·31	0·37	0·53	0·14	0·20	21·32	21·12
Na_2O	0·02	0·00	0·04	0·00	0·30	0·03	0·00	0·00	0·47	0·47
K_2O	0·00	0·07	0·00	0·00	0·00	0·00	0·00	0·00	0·00	0·00
Cr_2O_3	—	—	0·10	0·01	—	0·00	0·02	0·02	—	—
Total	99·76	99·46	100·00	99·94	100·42	99·05	98·30	99·37	99·44	99·32
Cations on the basis of 6 oxygens										
Si	1·930	1·869	1·867	1·726	1·656	1·688	1·663	1·674	1·927	1·931
Ti	0·005	0·007	0·006	0·002	0·008	0·025	0·001	0·004	0·014	0·013
Al	0·063	0·243	0·322	0·508	0·601	0·544	0·621	0·646	0·110	0·109
Fe	0·604	0·712	0·636	0·819	0·692	0·702	0·823	0·805	0·256	0·257
Mn	0·010	0·003	0·005	0·022	0·009	0·011	0·014	0·007	0·005	0·004
Mg	1·375	1·153	1·166	0·909	1·000	1·007	0·874	0·856	0·821	0·823
Ca	0·045	0·009	0·005	0·013	0·015	0·021	0·006	0·008	0·854	0·846
Na	0·001	—	0·003	—	0·021	0·002	—	—	0·034	0·034
K	—	0·004	—	—	—	—	—	—	—	—
End-members										
Wo	2·20	0·50	0·29	0·71	0·85	1·22	0·33	0·49	44·07	40·23
En	67·46	61·41	64·33	51·60	58·30	57·84	50·92	51·05	42·39	47·10
Fs	30·34	38·10	35·38	47·69	40·85	40·93	48·75	48·46	13·54	12·67

impure composition are typical of those zones around mafic minerals where partial melting has occurred (Grapes, 1985).

GEOCHEMISTRY OF THE PERALUMINOUS GRANULITIC XENOLITH SUITE

Major elements

Major and trace element data for 18 whole-rock samples are given in Table 3. For the small charnockitic xenoliths, no powder was available for bulk chemical analysis.

All the analysed xenoliths are strongly peraluminous in composition, with the pelitic xenoliths showing higher A/CNK values (1·3–1·1) than the felsic types (A/CNK 1·2–2·2) (Fig. 6). From their SiO_2 content, some pelitic xenoliths are ultrabasic or basic rocks (e.g. sample U-10, which is almost entirely composed of garnet and sillimanite, has 36 wt % SiO_2, Table 3). Felsic xenoliths are always intermediate or acid in composition (Fig. 6). Pelitic xenoliths are characterized by low Na_2O ($\leq 1{\cdot}2$ wt %) and CaO ($\leq 1{\cdot}1$ wt %) contents, and also by higher Al_2O_3, TiO_2 and Fe_2O_3t than felsic ones, and have lower MgO contents (Fig. 6). K_2O contents are high in both types, with the exception of sample U-10 with only

Table 2: Representative electron microprobe analyses (V)

	Phlogopite					
Xenolith type:	2a	2b	2b	2b	2b	2b
Sample:	81846	81841	95151	95148	99193	U-49
Analysis no.:	14	23	18	14	2	
SiO_2	37·91	36·80	37·44	38·29	37·54	37·99
TiO_2	6·45	5·95	5·93	4·99	6·56	4·97
Al_2O_3	15·34	15·05	13·96	14·35	13·49	15·67
FeO	11·20	11·19	9·93	7·63	9·90	10·02
MnO	0·02	0·05	0·10	0·04	0·03	0·05
MgO	14·48	15·69	18·96	18·12	16·64	16·46
CaO	0·00	0·00	0·02	0·00	0·00	0·01
Na_2O	0·32	0·38	0·29	0·45	0·61	0·49
K_2O	8·87	10·72	8·86	9·79	9·01	9·44
F	2·06				3·19	
Total	96·65	95·83	95·49	93·66	96·96	95·09
$-O \equiv F$	−0·87	—	—	—	−1·34	—
Total	95·78	95·83	95·49	93·66	95·69	95·09
Cations on the basis of 22 oxygens						
Si	5·575	5·428	5·451	5·632	5·571	5·548
Ti	0·714	0·660	0·650	0·552	0·732	0·546
Al	2·657	2·613	2·393	2·485	2·358	2·695
Fe	1·377	1·380	1·209	0·939	1·229	1·224
Mn	0·002	0·006	0·012	0·005	0·004	0·006
Mg	3·175	3·451	4·116	3·973	3·682	3·584
Ca	—	—	0·003	—	—	0·002
Na	0·091	0·108	0·080	0·128	0·175	0·139
K	1·664	2·018	1·645	1·837	1·705	1·759

0·72 wt %. In spite of their heterogeneous nature, the peraluminous granulites show marked trends of decreasing Al_2O_3, Fe_2O_3t, TiO_2 and MgO with SiO_2 content of the rock, although they define parallel 'suites' in some diagrams (e.g. MgO vs SiO_2 diagram, Fig. 6).

Trace elements

Pelitic xenoliths have higher contents of some transition metals (Cr, Sc and V), high field strength elements (HFSE; Nb, Y) and heavy REE (HREE) compared with felsic xenoliths (Fig. 7), reflecting their higher garnet and rutile contents. The strongly peraluminous metapelite U-10 is highly depleted in large ion lithophile elements (LILE) and light REE (LREE) with respect to the rest of the xenolith suite (Fig. 7). When normalized to average continental crust (Fig. 8), the pelitic xenoliths show a two-fold enrichment in some LILE such as Rb, Ba and K. This kind of xenolith also shows a negative anomaly in Sr and a less marked one in Zr. Felsic granulites also show negative Th and Nb anomalies (Fig. 8).

REE patterns, except that of xenolith U-10, are LREE enriched and have negative Eu anomalies, although some felsic xenoliths have no Eu anomaly or a positive one (Fig. 9). The latter is related to the abundance of feldspars in this kind of xenolith. The most mafic xenolith U-10 has a flat REE pattern with a marked negative Eu anomaly. This REE pattern resembles that of mid-crust level garnets, which tend to lose their negative fractionation pattern compared with garnets of more epizonal levels, thus acquiring a flatter pattern (Bea, 1996). All analysed xenoliths are characterized by their high HREE content [even higher than in the estimated lower continental crust of Wedepohl (1995)]; they also show a slightly higher LREE content in comparison with estimated continental crust (Wedepohl, 1995).

Sr and Nd isotopic data

Measured Sr and Nd isotopic ratios for the xenoliths are given in Table 4. Isotopic ratios have also been calculated at 300 Ma, an average age for the Hercynian granite plutonism in the SCS (Villaseca *et al.*, 1995). In the age-corrected ε_{Nd} vs $^{87}Sr/^{86}Sr$ diagram (Fig. 10), pelitic and felsic xenoliths plot in different areas, the felsic ones having higher ε_{Nd} values (−8·2 to −1·4 with an average of −4·8) and lower $^{87}Sr/^{86}Sr$ ratios (0·70594–0·71300). These differences in isotopic compositions are very common when comparing felsic and pelitic types in lower-crustal xenolith suites (Downes & Leyreloup, 1986; Downes & Duthou, 1988; Eberz *et al.*, 1991). Of the three isotopic reservoirs defined by Downes (1993) for the lower continental crust in Europe (depleted mantle, ancient crust and felsic crust) the last component is dominant in the SCS xenolith suite. Differences in isotopic composition together with those found in major and trace element contents point to very different original sources for the two types of xenoliths.

Sample U-10 has very unusual age-corrected Sr and Nd isotopic ratios for SCS material, plotting towards fields typical of xenoliths from ancient terranes (Rudnick, 1992; Downes, 1993). This garnetiferous xenolith has a very high $^{147}Sm/^{144}Nd$ ratio (0·343), which is higher than in pelitic xenoliths both in the SCS and in other parts of the world (Downes & Leyreloup, 1986; Hanchar *et al.*, 1994).

DISCUSSION

P–T conditions

Mineral parageneses in granulitic xenoliths can provide information about the temperatures and pressures of the

Table 2: Representative electron microprobe analyses (VI)

	Ilmenite				Rutile				Sillimanite		
Xenolith type:	2a	2a	2b	2b	1	2b	2b	3	2b	3	3
Sample:	81846	81845	95151	99193	U-28	95151	99193	77750	95148	77750	U-46
Analysis no.:	17	129	2	26	8	159	12	3	5 inclus.	1	8
SiO_2	0·00	0·00	0·00	0·00	0·01	0·00	0·00	0·02	36·23	36·14	37·30
TiO_2	56·93	52·80	53·45	54·85	97·17	99·35	97·67	99·31	0·08	0·05	0·07
Al_2O_3	0·54	0·00	0·00	0·11	0·11	0·00	0·18	0·18	61·91	61·93	61·77
Cr_2O_3	0·08	n.d.	n.d.	0·00	n.d.	n.d.	0·00	0·04	n.d.	0·00	0·06
FeO	41·83	46·15	43·31	39·69	0·21	0·10	0·18	0·78	0·74	0·33	0·37
MnO	1·88	0·38	2·45	0·61	0·02	0·07	0·03	0·03	0·01	0·03	0·00
MgO	0·02	0·00	0·00	2·13	0·00	0·00	0·02	0·00	0·18	0·05	0·05
CaO	0·01	0·04	0·05	0·02	0·02	0·01	0·03	0·00	0·03	0·04	0·01
Na_2O	0·00	0·00	0·00	0·00	0·01	0·02	0·00	0·00	0·04	0·02	0·00
Total	101·28	99·37	99·25	97·41	97·56	99·55	98·09	100·38	99·22	98·59	99·62
	Cations per 6 O				*Cations per 2 O*				*Cations per 20 O*		
Si	—	—	—	—	—	—	—	—	3·959	3·965	4·045
Ti	2·084	2·013	2·031	2·070	0·997	0·998	0·996	0·993	0·006	0·004	0·006
Al	0·031	—	—	0·007	0·002	—	0·003	0·003	7·967	8·002	7·891
Cr	0·003	—	—	—	—	—	—	—	—	—	0·005
Fe	1·702	1·956	1·830	1·665	0·002	0·001	0·002	0·009	0·067	0·030	0·034
Mn	0·077	0·016	0·105	0·026	—	0·001	—	—	0·001	0·003	—
Mg	0·001	—	—	0·159	—	—	—	—	0·029	0·008	0·008
Ca	0·001	0·002	0·003	0·001					0·003	0·004	0·001
Na	—	—	—	—	—	0·001	—	—	0·009	0·005	—

last equilibration. The SCS xenoliths show no record of pre-granulitic episodes or evidence of polyphase metamorphism. However, low-*P* high-*T* effects related to transport in the lamprophyric dyke and subsequent hydrothermal metamorphism are superimposed on the granulitic parageneses.

The absence of osumilite, cordierite and kyanite in the peraluminous granulites implies pressures of 7–12 kbar for temperatures in the range of 800–900°C (Holdaway, 1971; Carrington & Harley, 1995), but this has to be regarded as a crude approximation because of the Fe-rich character of the xenoliths. In any case, the high modal amount of pyrope-rich garnet is consistent with the presence of abundant prismatic rutile crystals in all the peraluminous xenoliths, which is typical of high-pressure conditions in these compositions (Patiño Douce & Beard, 1995; Patiño Douce, 1996). The almost complete absence of mica in most xenoliths, with the exception of accessory phlogopite found in some felsic xenoliths, indicates that biotite dehydration-melting reactions have almost run to completion. Data from experiments with natural starting materials (pelites, greywackes, biotitic orthogneisses) at 5–10 kbar, have shown that at temperatures over 875–950°C, consumption of biotite is almost complete (Gardien *et al.*, 1995; Patiño Douce, 1996; Stevens *et al.*, 1997). This range of temperatures coincides with that of the appearance of orthopyroxene in peraluminous protoliths (Gardien *et al.*, 1995).

Several geothermometers and geobarometers were used to estimate the conditions of the last equilibration of the xenolith mineral assemblages (Table 5, Fig. 11). The lack of zoning in garnets and other mafic phases indicates attainment of equilibrium during granulitic conditions. Nevertheless, in all thermobarometric estimates, garnet cores were used, to avoid the possibility of rim recrystallization.

For the charnockitic granulites, temperatures calculated using Wells (1977) and Wood & Banno (1973) two-pyroxene thermometers gave similar results in the range of 930–960°C (Table 5). These are the highest temperatures recorded in the granulitic xenoliths. Estimated pressures of ~12 kbar were obtained from the

Table 2: Representative electron microprobe analyses (VII)

	Spinel							
Xenolith type:	2a	2b	2b	2b	2b	2b	3	3
Sample:	81846	95151	95151	99193	99193	99185	77750	U-46
Analysis no.:	3	5	1	13	28	26	18	24
				core	rim			
SiO_2	0·09	0·00	0·04	0·05	0·08	0·37	1·14	0·36
TiO_2	0·02	0·06	0·24	0·82	0·68	0·8	0·02	0·32
Al_2O_3	63·13	63·55	62·25	60·63	61·01	62·12	60·20	57·84
Cr_2O_3	0·16	n.d.	n.d.	0·32	0·09	0·15	0·07	0·07
FeO	27·47	26·77	27·80	24·27	29·12	26·44	28·96	34·10
MnO	0·27	0·16	0·24	0·13	0·17	0·27	0·19	0·15
MgO	9·22	9·98	8·72	12·44	7·60	9·68	6·90	5·47
CaO	0·02	0·00	0·06	0·00	0·04	0·05	0·01	0·01
Na_2O	0·00	0·00	0·00	0·00	0·00	0·00	0·01	0·02
ZnO	0·07	n.d.	n.d.	0·79	0·00	0·00	0·29	0·03
Total	100·44	100·52	99·37	99·44	98·78	99·16	97·79	98·42
Cations on the basis of 32 oxygens								
Si	0·019		0·009	0·011	0·017	0·079	0·253	0·081
Ti	0·003	0·010	0·039	0·133	0·113	0·012	0·003	0·054
Al	15·962	15·979	15·950	15·392	15·853	15·851	15·786	15·525
Cr	0·026			0·054	0·016	0·025	0·012	0·013
Fe	4·932	4·780	5·058	4·374	5·374	4·791	5·392	6·499
Mn	0·049	0·029	0·043	0·023	0·032	0·050	0·035	0·029
Mg	2·952	3·175	2·828	3·996	2·498	3·127	2·290	1·859
Ca	0·005	—	0·014	—	0·009	0·012	0·003	0·003
Zn	0·010	—	—	0·130	—	—	0·050	—
Na	—	—	—	—	—	—	0·003	0·009

cpx–plg–qtz geobarometer of Ellis (1980). However, this charnockitic granulite is quartz free, so the pressure thus obtained is a maximum value as silica activity is less than unity.

Orthopyroxene-bearing peraluminous granulites (samples 81845 and 81846, Table 5) also gave high T estimates (870–910°C) with the grt–opx geothermometer of Harley (1984) for pressures around 9–11 kbar. Garnet–biotite equilibria yielded consistent temperatures around 900–1000°C (Table 5). Phlogopite-bearing peraluminous granulites gave temperatures in the range 800–900°C with garnet–biotite thermometers (Hodges & Spear, 1982; Hoinkes, 1986), in agreement with the experimental data on the stability of biotite in melting experiments. The calibration by Ferry & Spear (1978) gave results 50–70°C lower than other calibrations of the garnet–biotite thermometers. Pressures calculated using GRIPS (Bohlen & Liotta, 1986) and GASP (Ganguly & Saxena, 1984) geobarometers were 6·5–10 kbar, slightly lower than other estimates in related xenoliths.

Two-feldspar thermometry agrees with the high T estimations, as can be seen from the projection of the mineral compositions in the Ab–An–Or diagram with isotherms at 5 kbar after Fuhrman & Lindsley (1988) (Fig. 3). The high anorthite content in the alkali feldspar (5–10%) and of orthoclase in plagioclase (up to 20%) indicates high-T equilibration in the range 800–900°C.

These results suggest that the granulitic xenoliths last equilibrated in the lower crust within a depth range of 23–38 km. Such depths are in good agreement with geophysical data concerning the crustal structure of central Spain, particularly the estimates of Moho depth (30–32 km).

Superimposed on the granulitic parageneses is a recrystallization assemblage, which is the result of the transport of the xenoliths in the lamprophyric magma.

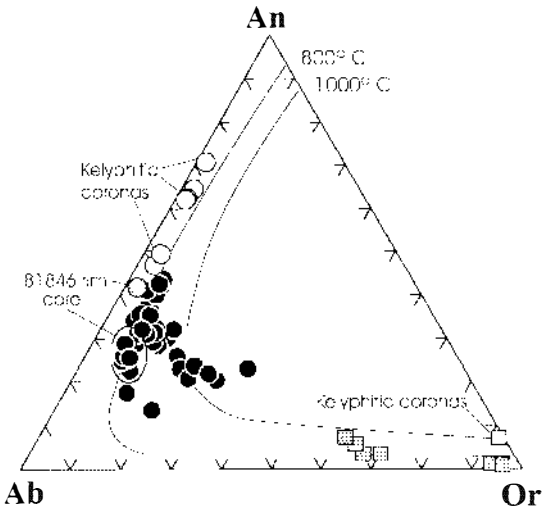

Fig. 3. Ternary feldspar diagram showing the composition of plagioclase (indicating kelyphitic and symplectite rims varieties) and alkali feldspar of the granulitic xenoliths. Also shown is the location of the isotherms 800 and 1000°C at 5 kbar of Fuhrman & Lindsley (1988).

Kelyphitic coronas are decompressional features and not the result of polyphase metamorphism, as has been demonstrated in other xenolith suites (Rudnick, 1992). The low-pressure orthopyroxene–spinel corona is formed at very high temperatures (up to 1200°C) as deduced from the results of the garnet (rim)–orthopyroxene (kelyphitic) equilibrium (Table 5). Some outer coronas that are composed of chlorite and opaque minerals indicate hydrothermal recrystallization related to the subvolcanic emplacement of the lamprophyre dyke (Rudnick, 1992). The *P–T* evolution of the xenolith suite, with the calculated decompression path, is summarized in Fig. 11.

Heat productivity of the SCS lower crust

The abundances of heat-producing elements (HPE) in granulite xenoliths and granulite terranes are crucial for estimating the composition of the lower continental crust (McLennan & Taylor, 1996). On the basis of continental heat flow data, McLennan & Taylor made an evaluation of the K, Th and U contents of the average continental crust; K_2O must be ~1·3 wt %, Th ~4·2 ppm and U ~1·1 ppm. These values are lower than those recently published by Wedepohl (1995), which are 2·4 wt %, 8·5 ppm and 1·7 ppm, respectively. For the lower crust the estimates are 1·6 wt %, 6·6 ppm and 0·93 ppm, respectively (Wedepohl, 1995).

Felsic and pelitic xenoliths from the SCS (excluding sample U-10) have average values of HPE of 3·4 wt % K_2O, 5·0 ppm Th, and 0·47 ppm U, and of 4·0 wt %

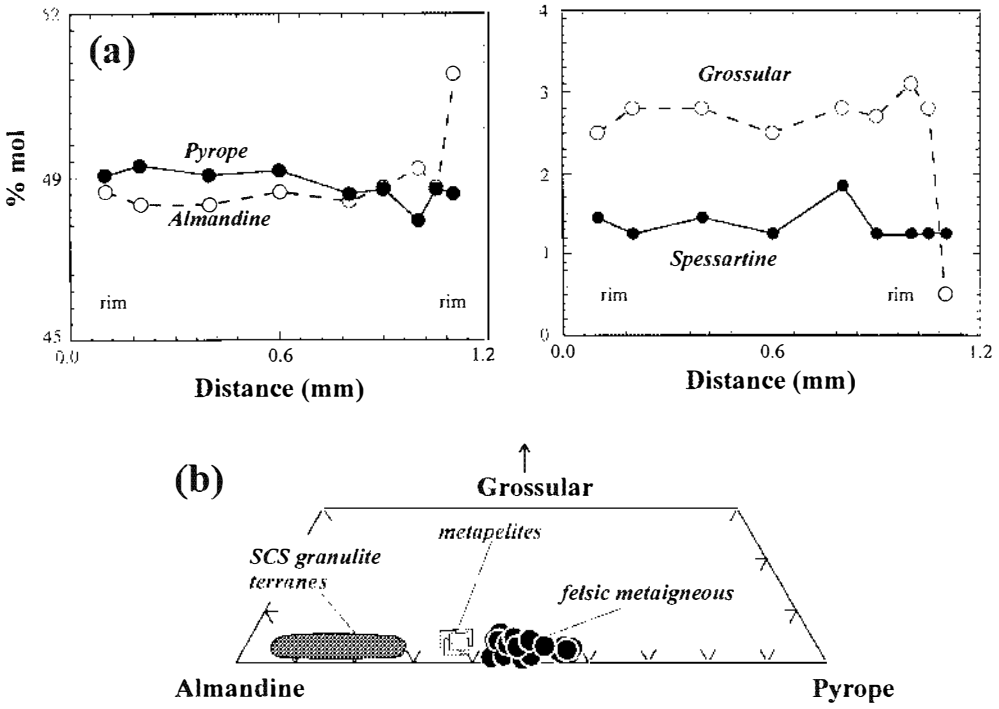

Fig. 4. (a) Electron microprobe traverse through garnet in a felsic xenolith (sample 95151). (b) Relative proportions of end-member molecules for garnets in granulitic xenoliths. Garnets from granulites and migmatites of the regional granulitic terrane of Toledo (Barbero, 1995) are also shown for comparison.

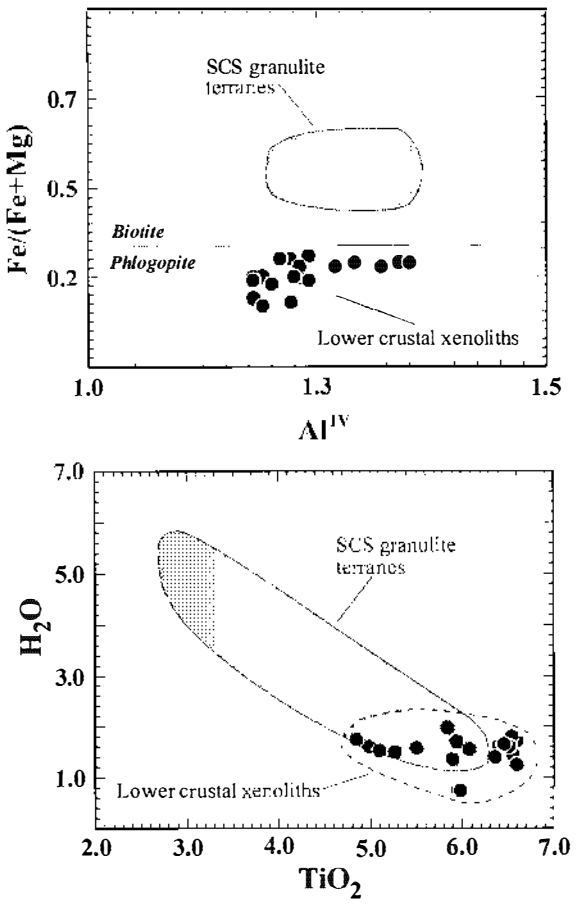

Fig. 5. Chemical composition of phlogopite from granulitic xenoliths in comparison with that of biotites from the regional granulitic terrane of Toledo (Barbero, 1995). H_2O content in mica is estimated by the method of de Bruiyn *et al.* (1983).

K_2O and 15·4 ppm Th, respectively (Table 3). No U data are yet available for the pelitic xenoliths. With these HPE contents we have calculated the radioactive heat productivity using heat productivity rates for K, U and Th from Rybach & Muffler (1981). Values of 0·79 μW/m^3 for felsic xenoliths and 1·67 μW/m^3 for pelitic types are obtained for the SCS lower crust. These values are close to the average lower continental crust value (0·90 μW/m^3) proposed by Wedepohl (1995), but are higher than the values of Rybach & Muffler (1981) (0·45 0·73 μW/m^3) and those of average xenolith suites of Rudnick (1992) (0·28 μW/m^3), or for the average continental crust estimated by McLennan & Taylor (1996) (0·71 μW/m^3). The estimated values of HPE for the SCS lower crust are much higher than those used in theoretical models of anatexis in tectonically thickened continental crust (England & Thompson, 1986; Patiño Douce *et al.*, 1990). Moreover, this high crustal radioactive heat production has to be considered in addition to the magnitude of thickening in the SCS during the Hercynian orogeny, which is estimated to have been more than twice the initial pre-Hercynian crust [Villaseca *et al.* (1998) and references therein]. Considering these parameters in thermal models, heat production rates in the SCS are high enough to raise the temperature to >900°C at the base of the crust, without any increase in the basal heat flux. This thermal productivity of the lower crust is high enough to promote extensive melting and thus can explain granite generation in the SCS during the Hercynian orogeny.

Restitic character of the SCS lower crust: implications for Hercynian granite genesis

The modal mineralogy of the granulitic xenoliths is consistent with a residual character for most of them. Sample U-10 (Tables 1 and 3), which is exclusively composed of garnet and sillimanite, is more mafic in composition than some pelitic granulites used in experimental studies, which do not yield significant melt until temperatures >1000°C are reached (Beard *et al.*, 1993). The low proportion of mica in the SCS xenoliths could be a consequence of biotite dehydration-melting reactions. The abundance of modal K-feldspar in most xenoliths does not contradict the possibility of a residual character after granitic melt extraction. As stated by Carrington & Watt (1995), consumption or production of K-feldspar in biotite dehydration-melting reactions is highly dependent on the H_2O/K_2O ratio of the melt and K-feldspar production is enhanced at higher pressures. Moreover, incomplete separation of the high-viscosity granitic melt could also give rise to a feldspar-rich residue, as argued for other lower-crustal granulites (Rudnick & Presper, 1990; Schnetger, 1994).

The major element chemistry of the pelitic xenoliths (Al_2O_3 > 25 wt %, FeO_t > 10 wt %, MgO > 3 wt %) is consistent with these xenoliths being melting residua. They plot in more mafic and Al-rich fields than pelitic parents as would be expected from a mass balance approach of partial melting of metasediments from which a granite melt was removed (MacRae & Nesbitt, 1980) (Fig. 12). Nevertheless, the difference in isotopic composition from the Hercynian granitoids and their relative scarcity in the xenolith suite suggest a minor contribution of this type of source in the genesis of the SCS granites. This corroborates other geochemical approaches to granite petrogenesis in the area (Villaseca *et al.*, 1998).

In Fig. 12 a crude linear array connects felsic xenoliths and Hercynian granites from the SCS, passing through the composition of the outcropping orthogneisses. Such linearity would be expected to occur when removing granitic liquid from orthogneissic rocks (see CNW path in Fig. 12). This process tends to produce more Al-, Fe- and Mg-rich restites, whose composition must be located

Table 3: Major (wt %) and trace element (ppm) composition of the SCS xenolith suite

	Felsic metaigneous													Metapelites				
Sample:	U-141 81846	U-50	U-152 95148	U-49	U-156 95152	U-155 95151	U-157 95153	U-145 95141	U-92 77747	U-147 95143	U-146 95142	U-93 77748	U-153 95149	U-10	U-90 77745	U-91 77746	U-42	U-96 77750
SiO_2	61·35	53·47	58·57	60·12	61·01	62·15	62·4	62·96	63·05	63·24	65·96	67·42	68·38	35·9	46·71	46·85	49·41	55·02
TiO_2	0·89	1·45	1·02	1·01	0·89	1·17	1·11	1·05	1·04	0·98	0·81	0·61	0·83	2·11	1·50	1·38	1·27	1·28
Al_2O_3	15·48	18·10	17·52	18·06	18·68	16·29	16·11	16·56	16·44	15·50	15·69	15·80	15·16	34·11	27·53	26·01	24·79	24·72
Fe_2O_3	8·04	10·57	8·87	8·21	7·29	8·65	8·55	8·96	8·15	9·12	6·55	4·50	6·00	17·00	12·37	12·70	11·21	9·94
MnO	0·13	0·10	0·07	0·10	0·12	0·09	0·11	0·09	0·11	0·13	0·08	0·03	0·09	0·12	0·12	0·09	0·05	0·06
MgO	3·48	4·05	3·49	3·34	3·43	4·80	4·10	3·69	3·18	4·66	2·76	1·75	2·53	4·78	3·42	3·32	3·01	2·29
CaO	2·83	1·33	1·25	1·40	2·39	1·80	1·75	0·89	0·98	1·17	0·77	2·11	2·01	0·95	0·62	1·09	0·64	0·41
Na_2O	3·07	4·14	2·16	2·80	3·21	2·20	2·38	1·79	3·19	1·36	2·23	2·82	2·84	0·36	1·16	0·97	0·46	0·63
K_2O	2·26	4·98	4·44	3·31	2·76	2·09	2·46	2·93	3·38	4·02	5·01	4·20	1·72	0·72	4·06	4·53	3·87	3·42
P_2O_5	0·17	0·27	0·12	0·27	0·12	0·09	0·07	0·11	0·31	0·20	0·07		0·07	0·16	0·24	·	0·13	0·13
LOI	2·03	2·78	2·12	1·55	0·79	0·74	1·07	0·70	1·29	—	2·14	1·48	1·00	3·59	2·61	2·44	4·25	1·76
Total	99·73	100·43	99·63	99·61	100·7	100·08	100·11	99·73	100·56	100·37	102·05	100·8	100·63	99·8	99·57	99·55	99·59	99·66
Ba	596	1435	1075	1175	747	768	915	646	864	1300	1305	1688	436	263	1272	996	1362	929
Rb	58	119	99	88	74	52	64	82	45	122	151	155	53	60	126	130	148	108
Sr	258	252	224	281	409	247	282	147	98	440	419	432	315	76	233	162	151	141
Ga	18		23		20	16	17	20		15	16		18	48			24	33
Ta			1·9		2·2	2	1·9	2·5		3·4	1·7		1·2					
Nb	13		14		18	15	17	12		15	16		9	35			23	21
Zr	212	200	282	202	221	224	211	237	158	169	213	157	203	222	91	174	173	247
Y	32	38	30	45	47	48	44	42	35	47	35	34	36	75	59	36	42	46
Th	10	8	8	4	13	2	3	2			1	3	5	2	6		19	22
U			0·83		1·05	0·30	0·28	0·39			0·12		0·29					
Cr	301		236		99	127	129	264		151	107		94	403			475	246
Ni	60	70	147	97	75	55	23	36	45	72	72	56	41	57	68	76	103	36
Co	19		27					20						24			25	20
Sc	12		10					12						26			15	12
V	131		145		93	162	165	168		152	97		103	331			159	156
Cu	7		99		55	32	20	5		44	74		22	25			80	16
Zn	71		54		78	86	121	101		93	60		65	178			77	98
La	38·85		52·34	41·75		33·90	37·50	32·42		30·30	34·40			11·56	30·21		55·98	68·14
Ce	74·31		94·98	86·40		64·99	72·22	62·80		59·14	63·18			24·21	52·70		99·15	130·90
Nd	31·05		37·20	38·08		26·36	27·80	30·72		27·00	22·06			16·02	19·64		46·04	63·95
Sm	5·95		7·17	8·38		6·02	6·14	7·22		6·64	4·07			9·09	7·26		9·45	11·80
Eu	1·56		2·27	1·83		1·82	1·75	1·48		1·50	1·88			0·63	2·30		1·94	2·24
Gd	5·78		7·01	7·04		6·83	7·08	7·14		7·80	4·65			13·62	8·84		8·64	9·05
Dy	5·47		5·56	6·80		7·67	7·41	6·18		8·20	5·52			13·01	9·80		7·30	7·59
Er	3·22		2·79	3·82		4·55	4·05	4·26		4·45	3·08			7·25	4·77		4·12	4·45
Yb	3·60		2·90	3·77		4·44	4·25	4·70		4·43	3·13			7·44	4·47		4·34	4·33
Lu	0·56		0·44	0·62		0·78	0·75	0·67		0·77	0·54			1·08	0·70		0·62	0·60

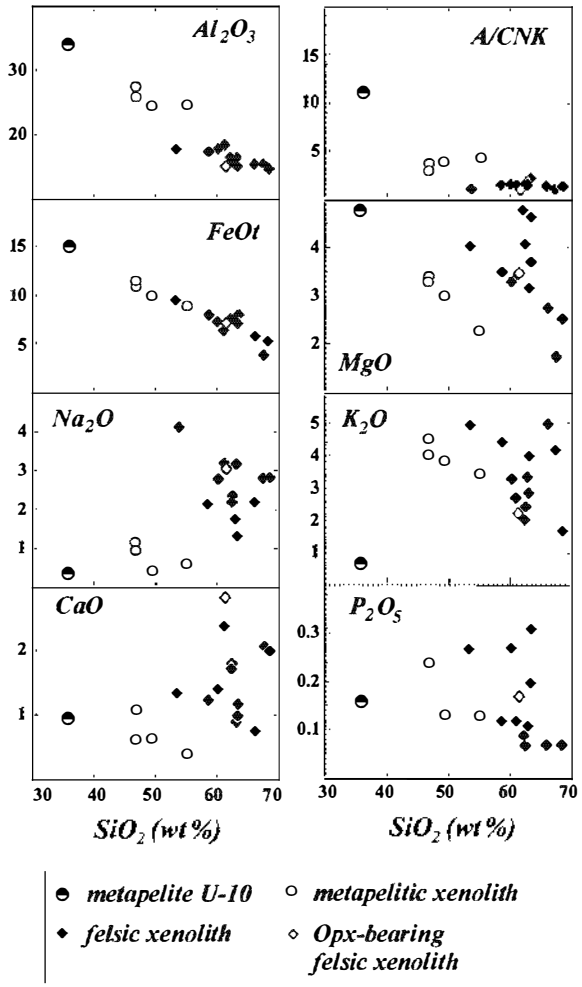

Fig. 6. Harker plots showing the variation of major elements in the granulitic xenoliths. Major element data in wt %. A/CNK is the molar ratio of Al_2O_3 to the sum (K_2O + Na_2O + CaO).

at the ends of the lines projecting through SCS granites and orthogneisses (see inset in Fig. 12a). Most of the felsic xenoliths do indeed plot at the end of this linear array (Fig. 12). Moreover, a complementary character in major and trace element composition, between some felsic meta-igneous xenoliths and the granites, is observed (Figs 12 and 13). This is particularly notable when considering LILE (Rb, K, Ba, Sr) and some transition metals (Sc, V, Ni). Those trace elements controlled by accessory phases (i.e. REE, except Eu, and HFSE) do not fit the mass balance so well.

To test the hypothesis that the felsic granulitic xenoliths represent residua after granitic melt extraction, with the melts being represented by the Hercynian plutons, major and trace element mass balance modelling has been performed. In this modelling an orthogneissic protolith rather than a pelitic one has been selected, as previously discussed.

Table 6 shows that, considering an average SCS orthogneiss as the protolith for the granites, it is possible to obtain melting residua whose compositions are very similar to that of the average meta-igneous xenoliths. We have calculated the composition of the restitic lower crust after subtraction of variable (29–33%, Table 6) granitic partial melts of known composition (columns 1–4, Table 6) from the average orthogneissic protolith. The calculated residua (columns 7–11, Table 6) have a major and trace element composition close to that of the average felsic meta-igneous xenolith (column 6, Table 6). The goodness of the fit is reflected in the calculated R^2 residuals (0·96–2·19); also the calculated degree of melting of ~30% supports this possibility. The proportion of melt obtained in dehydration-melting experiments at ~900°C and 10 kbar from meta-igneous protoliths (biotite gneisses) is ~10–30% (Skjerlie & Johnston, 1993; Gardien *et al.*, 1995; Patiño Douce & Beard, 1995) which agrees with the degree of melting calculated in our mass balance modelling. In Fig. 14a we have plotted the major and trace element composition of the calculated residua after the mass balance calculation and of the sampled felsic meta-igneous xenoliths.

We further tested our hypothesis that the felsic xenoliths are residues of melting by estimating the trace element concentration using batch melting equations and published partition coefficients (see Appendix B, Table B1 and references therein). This modelling is hindered by the availability of partition coefficients and also by the fact that several trace elements, especially the REE, reside in accessory phases whose abundances and behaviour are generally poorly constrained. Nevertheless, for Ba, Rb, Sr and REE, the compositions of residues after partial melting of orthogneissic sources have been calculated (columns 12–14, Table 6) and also plotted in Fig. 14a with previous models. In the modelling, both modal and non-modal batch melting calculations have been performed, giving similar results (see models 12 and 13 in Table 6). The main difference between models 13 and 14 is the involvement of monazite in both the melt and restite assemblages, necessary to account for the observed LREE contents in xenoliths (Fig. 14a). Biotite is the first mineral to disappear, as shown by the modal depletion in the SCS xenoliths compared with equivalent protoliths in outcropping granulitic terranes. Biotite is also the first mineral substantially consumed in melting experiments in biotite gneisses, with the remaining quartz or plagioclase being very close to their initial modal proportions (Gardien *et al.*, 1995; Montel & Vielzeuf, 1997). Similarly, minerals produced in the melting reaction, garnet and K-feldspar, are supposed to be more concentrated in restite assemblages. The calculated modal source composition after 30–35% of melting is 0·27 Qtz + 0·28 Kfs + 0·28 Plg + 0·15 Grt + 0·01 Bt. This closely

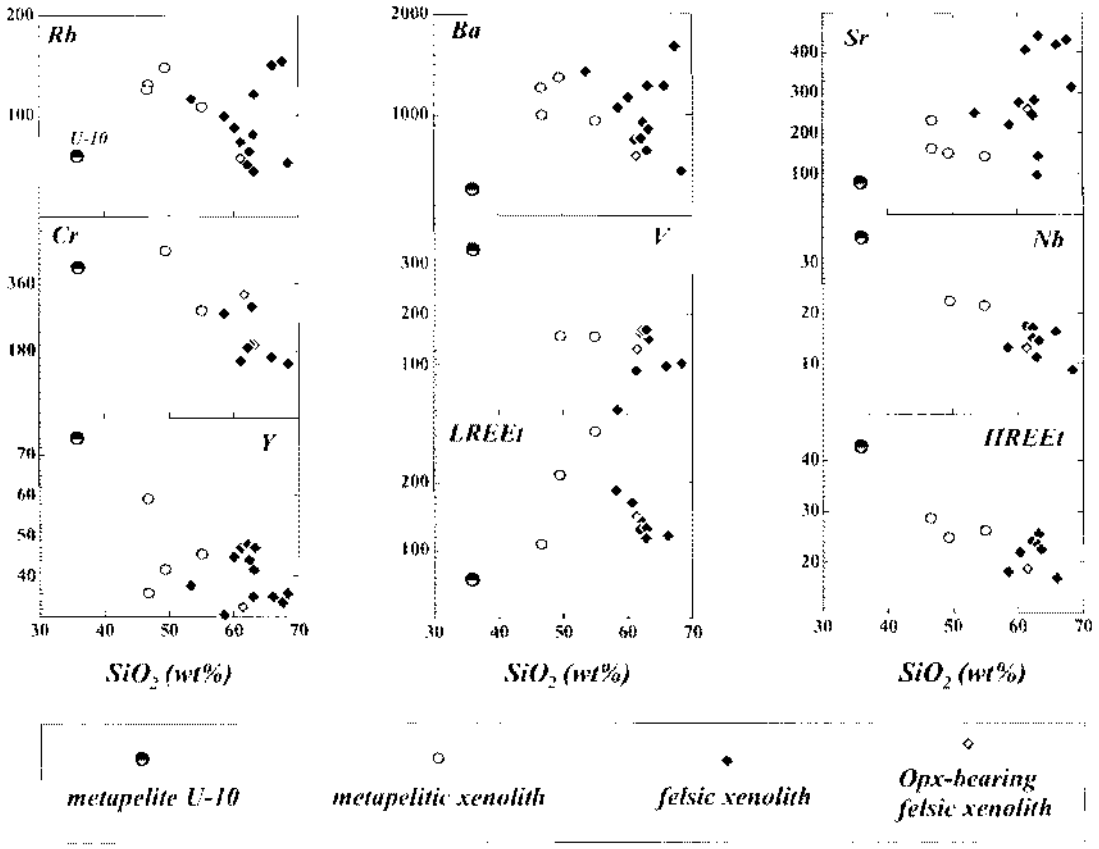

Fig. 7. Harker plots for trace elements in the granulitic xenoliths. Trace element data are given in ppm.

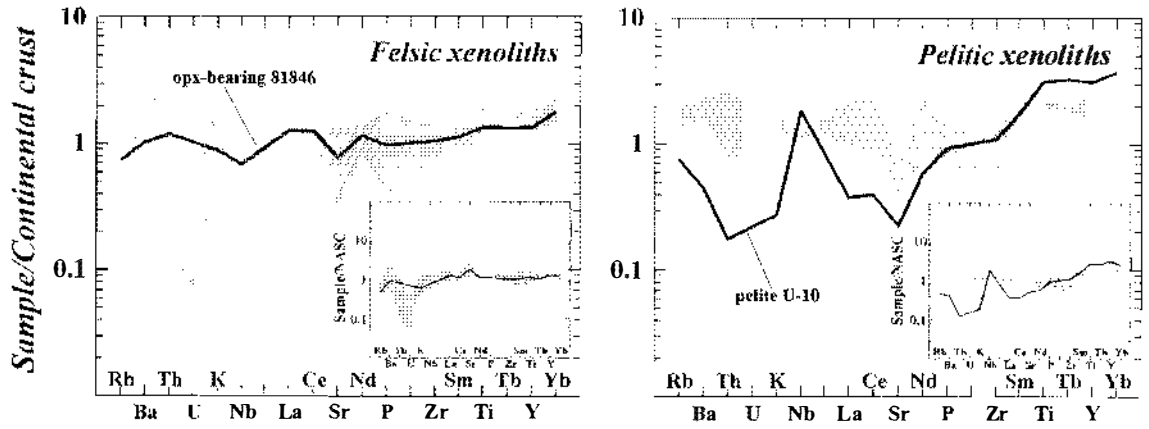

Fig. 8. Multi-element diagram of trace element normalized to the averaged continental crust of Wedepohl (1995), showing the geochemical characteristics of the two main types of granulitic xenoliths. Strongly depleted restitic xenolith U-10 and the orthopyroxene-bearing felsic xenolith 81846 are plotted separately. Inset shows trace element concentration normalized to North American Shale Composite (NASC) values (Gromet *et al.*, 1984).

resembles the modal assemblages of the SCS felsic xenoliths (Table 1). Modelled restite 14 is in the range of compositions of the SCS xenoliths (Fig. 14a), and changes in modal proportions of other major felsic phases in the melting reaction do not substantially modify the result.

Table 6 also shows the compositions of calculated

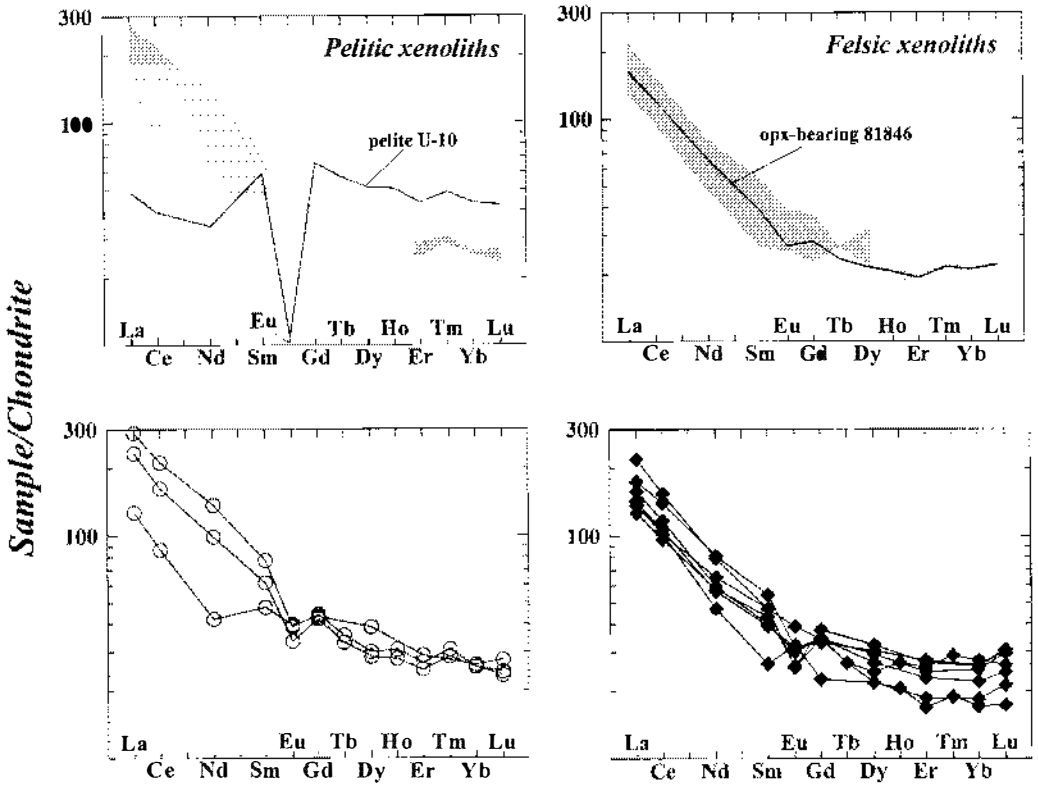

Fig. 9. Chondrite-normalized REE plots of granulitic xenoliths. In upper diagrams strongly restitic pelitic xenolith U-10 and orthopyroxene-bearing xenolith 81846 are plotted together with their respective compositional fields of related granulite-types. Chondrite values of Evensen *et al.* (1978).

liquids in equilibrium with the granulitic xenoliths as melting residues. The results (models 15 and 16 of Table 6) show a good fit to the compositions of the SCS granites for Ba, Rb, Sr and LREE (Fig. 14b). Departures in HREE and Y contents probably reflect modal variability of garnet in the source (a reduction from 10 to 5% in volume in the protolith broadly duplicates HREE concentration in the liquid) or the involvement of other accessory phases (e.g. zircon), but also might be the consequence of incomplete equilibration of garnet with the melt as melting and garnet production progress (Qiu, 1991; Miller *et al.*, 1992). Nevertheless, these results support the hypothesis of the granulitic xenoliths being melting residua after the extraction of liquids similar in composition to the SCS granites. The genetic relationship between the Hercynian peraluminous granites and the studied felsic metaigneous xenoliths is corroborated by the Sr and Nd isotopic composition of all these rocks. In Fig. 15, the Sr and Nd isotopic data of the lower-crustal xenoliths are plotted together with the isotopic data of SCS Hercynian peraluminous granites (Moreno-Ventas *et al.*, 1995; Pinarelli & Rottura, 1995; Villaseca *et al.*, 1998). The meta-igneous xenoliths match the isotopic composition of most of the peraluminous Hercynian granites, whereas the pelitic xenoliths have lower ε_{Nd} values, and plot outside of the granite field.

Crustal heterogeneity in terms of isotopic composition

The coincidence in Nd isotopes and the similar nature of the materials from SCS middle- and lower-crustal levels (dominantly meta-igneous and metapelitic lithologies) suggest that tectonic breaks do not exist between the middle- and lower-crustal levels as is the case in some other crustal segments (Eberz *et al.*, 1991). Nevertheless, Sr isotopic data of felsic meta-igneous and metapelitic xenoliths are closer to bulk Earth isotopic composition than those of orthogneisses and metapelites from shallower crustal levels (Fig. 10). As seen in other regions, there is a tendency for the Sr (and sometimes also Nd) isotopic composition of the lower continental crust to plot closer to bulk Earth values, whereas the upper-crustal levels tend to be more enriched (Downes & Duthou, 1988; Ruiz *et al.*, 1988; Eberz *et al.*, 1991). This tendency to greater isotopic homogenization, together with the lowering of Sr isotopic ratios, has also been

Table 4: Sr and Nd isotope data and concentrations (ppm) of the SCS granulite xenolith suite

Sample:	Rb	Sr	$^{87}Rb/^{86}Sr$	$^{87}Sr/^{86}Sr$	$^{87}Sr/^{86}Sr_{300Ma}$	Sm	Nd	$^{147}Sm/^{144}Nd$	$^{143}Nd/^{144}Nd$	$\varepsilon_{Nd(300)}$
Metaigneous										
U-50*	119	252	1·37	0·71546 ± 03	0·70961	10·0	52·0	0·1166	0·512198 ± 07	−5·6
U-49*	88	281	0·91	0·71514 ± 03	0·71126	7·67	39·4	0·1176	0·512209 ± 05	−5·4
U-92*	98	169	1·68	0·71815 ± 03	0·71098	6·47	29·2	0·1338	0·512383 ± 07	−2·6
U-93*	155	432	1·04	0·71038 ± 02	0·70594	6·94	34·5	0·1216	0·512423 ± 07	1·4
U-145†	97	186	1·51	0·71696 ± 01	0·71053	6·25	27·1	0·1396	0·512379 ± 08	2·9
U-146†	151	419	1·04	0·71182 ± 02	0·70739	4·07	22·1	0·1113	0·512167 ± 12	5·9
U-147†	122	440	0·80	0·70982 ± 01	0·70641	6·64	27·0	0·1487	0·512122 ± 05	−8·2
U-152†	85	240	1·03	0·71645 ± 01	0·71206	8·13	37·6	0·1307	0·512217 ± 07	−5·7
U-155†	52	247	0·61	0·71255 ± 01	0·70995	6·02	26·4	0·1378	0·512333 ± 04	−3·7
U-157†	64	282	0·66	0·71235 ± 01	0·70954	6·14	27·8	0·1335	0·512248 ± 04	5·2
U-141	58	258	0·65	0·71578 ± 06	0·71300	5·95	31·1	0·116	0·512074 ± 04	−7·9
Metapelites										
U-90*	126	233	1·57	0·72028 ± 03	0·71358	6·97	20·1	0·2101	0·512128 ± 07	10·5
U-91*	130	162	2·32	0·72030 ± 03	0·71040	6·99	20·5	0·2065	0·512150 ± 07	9·9
U-42	148	151	2·84	0·72164 ± 06	0·70951	9·45	46·0	0·124	0·511897 ± 03	−11·7
U-96	108	141	2·22	0·72694 ± 05	0·71746	11·8	64·0	0·112	0·511878 ± 03	−11·6
U-10	60	76	2·29	0·71465 ± 09	0·70488	9·09	16·0	0·343	0·512065 ± 18	−16·8

*Data from CNRS–UMR 6524 (Clermont-Ferrand, France).
†Data from Royal Holloway, University of London (UK).
Other data from CAI Geocronología y Geoquímica Isotópica of the Complutense University (Madrid). Sm and Nd concentrations were those measured by ICP-MS at the CNRS–CRPG Nancy. Errors in the concentration of these elements are <5%. Uncertainties for the $^{87}Sr/^{86}Sr$ and $^{143}Nd/^{144}Nd$ ratios are 2σ (mean) errors in the last two digits.

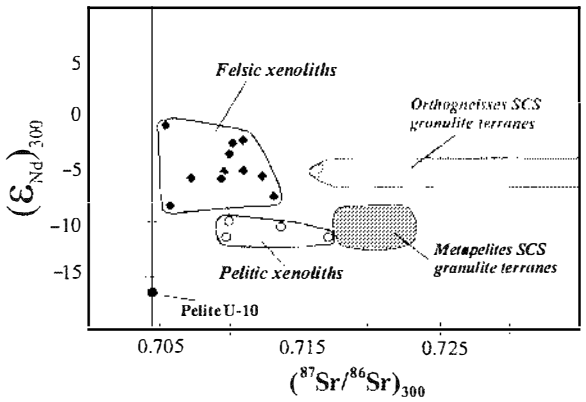

Fig. 10. ε_{Nd} vs $^{87}Sr/^{86}Sr$ at 300 Ma for the granulitic xenoliths. Fields for orthogneisses and metapelites at mid-crustal levels (Toledo and Sierra de Guadarrama) are taken from Villaseca *et al.* (1998).

observed in areas of progressive metamorphism (e.g. Central Pyrenees, Bickle *et al.*, 1988; eastern Nevada, Wickham, 1990). Several possibilities could explain this isotopic shift:

(1) Mixing processes with either the host magma or mixing with mantle-derived underplated material at the Moho or infracrustal levels (Downes & Leyreloup, 1986; Rudnick, 1992). Isotopic ratios of the SCS xenolith suite do not define a simple mixing array on the Sr–Nd isotope diagram (Fig. 10) and could be better interpreted as reflecting a diversity of sources for these rocks. Moreover, the marked peraluminous character of the xenoliths and their major and trace element compositions (the high Sr and Nd contents of the xenoliths make them less susceptible to contamination), together with the lack of significant basic underplating in Hercynian times (Villaseca *et al.*, 1998), rule out these possibilities.

(2) Isotopic changes related to the progressive metamorphism and associated anatexis. Bickle *et al.* (1988) invoked hydrous fluids generated during progressive dehydration of metamorphites as a mechanism to reduce and homogenize the Sr isotopic ratios in catazonal rocks in the Hercynian Pyrenees. Similar isotopic homogenization has been described in the Cooma complex (Chappell *et al.*, 1991), in Brittany and in eastern Nevada (Wickham, 1990). In all cases this modification is explained as resulting from fluid-mediated exchange with low $^{87}Sr/^{86}Sr$ rocks (e.g. carbonates) or pore fluids. The homogenization and lowering of isotopic ratios in crustal rocks during progressive metamorphism via fluid advection systems is also shown by other isotopic systems (Pb, O) (Wickham, 1990; McCulloch & Woodhead, 1993;

Table 5: Results of P–T estimates based on various geothermobarometers

Sample	Xenolith type	Temperature (°C)							Pressure (kbar)				
		grt–bt			grt–opx		opx–cpx		opx–grt		GRIPS	GASP	cpx–plg
		1 HS	2 H	3 FS		kelyph	1 WB	2 W	1 BNK	2 NP			
U-28	1						935	958					12
81846	2a	947	1000	910	870	1095				9·2	10		
81845	2a				910				9·36	11·0	10·5		
U-49	2b	790	825	750									
95148	2b	848	886	809							8	7·2	
81841	2b	887	953	866							8	8·5	
95151	2b	859	907	820		1280					6·5	7·5	
99185	2b					926					8·6	10·5	
99193	2b	835	895	801		1068					8·2	8·6	
77750	3a					990							

In all thermobarometric calculations, all iron was treated as Fe^{2+}. Garnet–biotite geothermometers: HS, Hodges & Spear (1982); H, Hoinkes (1986); FS, Ferry & Spear (1978). Garnet–orthopyroxene thermometry is from Harley (1984). Thermometers: WB, Wood & Banno (1973); W, Wells (1977). BNK, garnet–orthopyroxene geobarometer after Brey *et al.* (1986); NP, garnet–orthopyroxene–plagioclase–quartz geobarometer of Newton & Perkins (1982); GRIPS, garnet–rutile–ilmenite–plagioclase–quartz geobarometer of Bohlen & Liotta (1986); GASP, garnet–aluminium silicate–plagioclase geobarometer of Ganguly & Saxena (1984). The clinopyroxene–plagioclase–quartz geobarometer is after Ellis (1980).

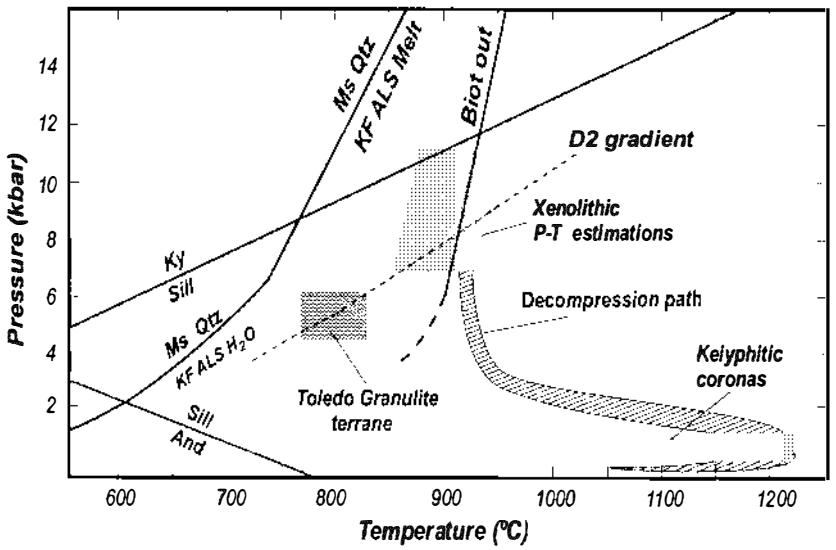

Fig. 11. *P–T* diagram for estimated granulitic conditions of lower-crustal xenoliths. *P–T* conditions of the regional granulitic terrane of Toledo (Barbero, 1995) and the estimated gradient during the Hercynian metamorphic peak of the sector are also shown. Kelyphitic coronas record the decompression and heating path followed by the xenoliths after rapid transport to shallow levels by the lamprophyric magma. Al_2SiO_5 curves after Holdaway (1971). Muscovite- and biotite-out curves are taken from Patiño Douce & Johnston (1991).

Holk & Taylor, 1997). Nevertheless, the absence of important carbonate layers in the metamorphic sequence of the SCS sector and the diminishing influence of pore fluids in the deepest crustal levels are obstacles to

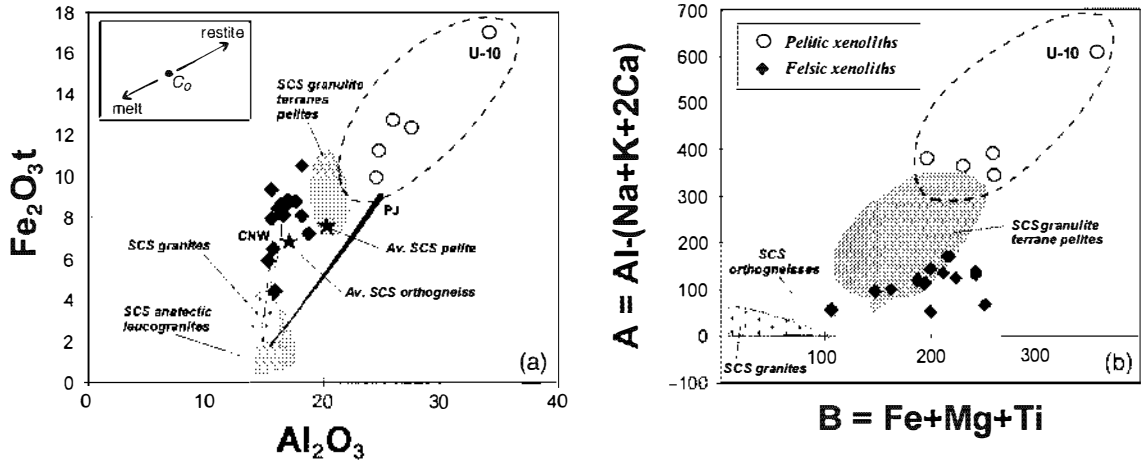

Fig. 12. Chemical plots based on major elements showing the restitic composition of the granulitic xenoliths. (a) A crude linear array between SCS granites and granulitic xenoliths across their respective protoliths is observed (see inset for interpretation of linear relationships). CNW is Conrad *et al.* (1988), path of melting meta-igneous protoliths that plot very close to the line connecting SCS granites and felsic granulites passing across the averaged SCS orthogneiss composition. Similarly, PJ is Patiño Douce & Johnston (1991) line connecting pelite with its experimentally obtained melts, suggesting by extrapolation a marked residual composition of the pelitic xenoliths. (b) A–B plot after Debon & Le Fort (1983). The parameters are in gram-atoms $\times 10^5$ in 100 g of rock. Hypothetical lines connecting SCS granites and outcropping orthogneisses and metapelitic rocks would show their corresponding granulitic xenolith plotted in expected restitic composition (see inset). (See text for further explanations.)

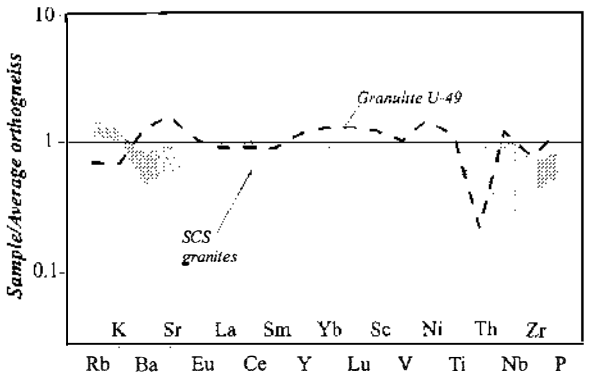

Fig. 13. Multi-trace element diagram normalized to average SCS orthogneiss for felsic U-49 granulite and SCS granites.

considering fluid mixing as the only mechanism to change Sr isotopic ratios. Therefore, in the lower crust, melting processes have to be involved together with this dehydration process. The lower crust is the section that has undergone the most extensive anatexis, suggesting that the anatectic melts themselves facilitated isotope exchange with the restites, and/or they served as a source of aqueous fluids that promoted such exchange. As isotopic interchange with externally derived aqueous fluids or granitic melts in catazonal rocks has been suggested in other localities (e.g. Wickham, 1990; Holk & Taylor, 1997), the main problem in our Hercynian crustal section is the origin of the low $^{87}Sr/^{86}Sr$ liquids or, on the contrary, the way to lose radiogenic strontium in processes affecting the lower crust. Further work is required to clarify the exact mechanism for this isotopic modification.

A more primitive isotopic composition of the lower continental crust was first envisaged by Taylor & McLennan (1985), who compared Sr–Nd isotopic data from granulite terranes (lower- to middle-crustal levels) with granulitic xenoliths that exhibit lower initial Sr ratios and higher initial Nd signatures. This tendency of lower-crustal granulites towards isotopically more primitive compositions has major consequences when evaluating the contribution of crustal sources in the genesis of granitic magmas. First, it can explain the apparent absence of the isotopically appropriate crustal protoliths in the outcropping metamorphic rocks, as has been discussed in several studies [the strontium paradox of Bernard-Griffiths *et al.* (1985) and Peucat *et al.* (1988); see also Clarke *et al.* (1988)]. The second consequence is that the important mantle contribution required by mixing models for some of the SCS granites which involve mantle-derived end-members and crustal materials (Moreno-Ventas *et al.*, 1995; Pinarelli & Rottura [redacted] can be severely reduced as the appropriate crustal component, as demonstrated here, has a more primitive Sr isotope composition.

Comparison with other Hercynian lower-crustal granulites from western Europe

Comparison of the composition of the lower crust of central Spain with that [redacted] her European Hercynian

Table 6: Major and trace element modelling: residual rocks after partial melting, melt fraction and melt composition

	1 Atalaya granite C_l-1	2 Navas granite C_l-2	3 Mora granite C_l-3	4 Alpedrete granite C_l-4	5 Average orthog. C_0	6 Average meta-igneous xenoliths C_s	7 Calc. Restite for C_l-1	8 Calc. Restite for C_l-2	9 Calc. Restite for C_l-3	10 Calc. Restite for C_l-4	11 Calc. Restite (C_s = U-49)	12 Residue Modal batch melting	13 Residue Non-modal batch melting	14 Residue Non-modal batch melting	15 Melt C_lNon-modal batch melting	16 Melt C_l (C_s/D) for U-49 as C_s
Melt (wt %)							33	29	32	31	32					
R^2							2·185	1·605	1·282	1·644	0·959					
SiO_2	68·08	70·44	70·19	70·07	63·66	60·77	60·18	60·06	60·06	60·07	60·97					
TiO_2	0·42	0·43	0·46	0·45	0·92	1·00	1·15	1·11	1·12	1·12	1·14					
Al_2O_3	15·80	14·88	15·52	15·39	16·99	17·06	17·23	17·62	17·52	17·50	17·78					
Fe_2O_3t	3·86	3·16	3·52	3·24	6·99	7·95	8·39	8·45	8·53	8·56	7·80					
MnO	0·04	0·05	0·06	0·05	0·07	0·08	0·08	0·08	0·08	0·08	0·08					
MgO	0·82	0·78	0·54	1·01	2·41	3·15	3·14	3·03	3·25	3·00	3·30					
CaO	3·25	2·02	2·16	2·38	1·66	1·27	0·84	1·49	1·41	1·32	1·43					
Na_2O	3·27	3·49	3·41	3·35	2·49	2·72	2·05	2·05	2·04	2·08	2·07					
K_2O	4·31	4·63	3·94	3·92	3·53	3·81	3·08	3·04	3·31	3·32	3·36					
P_2O_5	0·15	0·12	0·19	0·14	0·24	0·20	0·28	0·29	0·26	0·28	0·27					
Ba	765	502	559	494	949	959	1040	1132	1133	1153		1163	1120	1120	550	429
Rb	179	185	199	178	127	79	101	103	93	104		120	89	89	215	207
Sr	158	105	128	173	176	279	185	205	200	177		196	203	203	113	144
Y	30	25	33	24	40	41	45	46	43	47		51	53	53	10	9
La	54·94	27·53	26·74	28·03	50·73	40·87	48·7	60·2	62·0	60·9		19·7	21·6	46·8	59·8	35·8
Ce	113·55	58·91	58·19	58·45	107·17	78·58	104·0	126·9	130·2	129·1		40·0	45·9	98·0	128·6	76·4
Nd	48·79	27·45	27·76	27·16	48·46	32·10	48·3	57·0	58·2	58·0		16·0	18·4	42·2	63·1	37·3
Sm	9·22	5·62	6·15	6·06	10·12	6·73	10·6	12·0	12·0	11·9		5·5	6·5	9·3	11·9	7·8
Eu	1·25	0·96	1·14	0·94	1·75	1·85	2·0	2·1	2·0	2·1		2·1	2·2	2·2	0·8	0·7
Gd	6·96	4·63	5·62	5·18	8·85	6·75	9·8	10·6	10·4	10·5		8·1	9·0	9·4	7·6	5·2
Yb	2·74	2·21	2·85	2·00	2·96	3·79	3·0	3·3	3·0	3·4		3·9	4·0	4·0	0·6	0·6
Lu	0·39	0·30	0·37	0·31	0·48	0·63	0·5	0·6	0·5	0·6		0·6	0·6	0·6	0·1	0·1

Average orthogneiss is taken from Villaseca *et al.* (1993). Compositions of different peraluminous granites of the SCS are based on data from Villaseca *et al.* (1998). Average meta-igneous xenolith (C_s) is taken from the seven samples with $SiO_2 < 62·5$ wt % of Table 3. *Mass balance modelling*: 7–10 calculated restites, $C_s = (C_o - FC_l)/(1 - F)$. Calculated restite 11 for C_l-3 takes U-49 as C_s. *Batch melting modelling*: trace element compositions of residues after batch melting equations are $C_s = C_0D/[D(1 - F) + F]$ with $F = 0·3$ and modal estimation of the orthogneissic source as 0·25 Qtz + 0·25 Plg + 0·20 Kfs + 0·20 Bt + 0·10 Grt with K_d values of Table B1. D is the bulk distribution coefficient of the solid residue, and is the sum ($\Sigma X_i K_{di}$) where X_i is the weight fraction of each mineral and K_{di} is the crystal/liquid distribution coefficient for each mineral (Table B1). Residue 12 is calculated in the case of modal melting. Residue 13 is calculated non-modally with 0·55 Bt + 0·2 Qtz + 0·2 Pl + 0·05 Kfs entering the melt. Residue 14 is obtained as 13 involving 0·0002 Mnz in the source and 0·0004 in the melt. Trace element composition of melt 15 is the liquid in equilibrium with residue of model 14. Trace element composition of melt 16 is calculated as $C_l = C_s/D$ using U-49 as residual solid assemblage with D based on its modal mineralogy from Table 1 (0·43 Kfs + 0·31 Qtz + 0·10 Plg + 0·14 Grt + 0·01 Bt + 0·0002 Mnz) and K_d of Table B1.

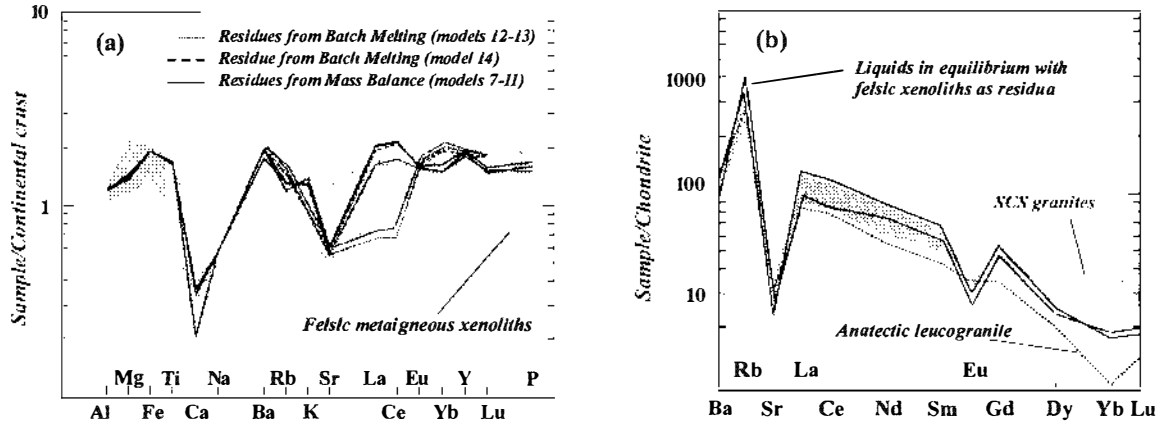

Fig. 14. (a) Major and trace element diagram normalized to average continental crust (Wedepohl, 1995). Calculated residues are taken from Table 6. (b) Trace-element chondrite-normalized diagram for SCS granites (Villaseca *et al.*, 1998), anatectic leucogranite of Toledo (Barbero *et al.*, 1995) and calculated liquids (continuous lines) in equilibrium with felsic xenoliths presumed to be their residual rocks. Liquid compositions are taken from Table 6 (columns 15 and 16).

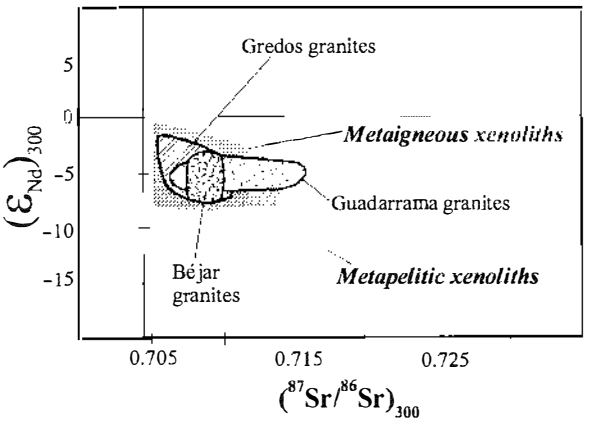

Fig. 15. Sr and Nd isotopic ratios at 300 Ma of granulitic xenoliths shown in comparison with SCS granites: Béjar sector (Pinarelli & Rotura, 1995), Gredos (Moreno-Ventas *et al.*, 1995) and Guadarrama (Villaseca *et al.*, 1998). Felsic meta-igneous and pelitic compositional fields of the xenoliths are drawn from Fig. 10.

areas reveals an important difference: in central Spain the lower crust is essentially felsic in character whereas in the French Massif Central (Downes & Leyreloup, 1986; Downes & Duthou, 1988) or in the Eifel volcanic region (Loock *et al.*, 1990) the lower crust contains an important component of mantle-derived basic material. With the exception of the granulitic xenoliths that appear in Cenozoic volcanic rocks in SE Spain (Sagredo, 1976; Vielzeuf, 1983; Cesare *et al.*, 1997), lower-crustal xenoliths are scarce elsewhere in Spain. In southeastern Spain metapelitic and charnockitic xenoliths from lower-crustal levels are described, their *P–T* estimates from phase equilibria being around 5–7 kbar, 700–850°C (Sagredo, 1976; Cesare *et al.*, 1997). These conditions are typical of middle- to lower-crustal levels. In any case, the absence of mafic metaluminous xenoliths in SE Spain reinforces the concept of a more felsic composition for the deeper crustal levels in the Iberia region.

Exposed granulite facies terranes can provide information on the lowermost crustal levels. The question of whether granulitic terranes are representative of the lower crust has been debated frequently (Downes, 1993). Some high-grade terranes are probably more representative of middle-crustal levels, as is the case for the granulite terranes in central Spain (Barbero, 1995) or the Agly massif in the Pyrenees (Pin, 1989). Other exposed granulite terranes from deeper crustal levels have been described in the Pyrenees (Saleix massif, Vielzeuf, 1984), Calabria (Maccarrone *et al.*, 1983) and northern Italy (Pin & Sills, 1986; Hermann *et al.*, 1997), and are undoubtedly representative of the lower continental crust. Data from these granulite facies terranes indicate a larger contribution of mantle-derived material, as in the Ivrea Zone (Pin, 1990; Voshage *et al.*, 1990), the Calabrian massif (Maccarrone *et al.*, 1983) and the Pyrenees (Pin, 1989). This suggests underplating of mantle-derived magmas at the base of the continental crust in these areas, in clear contrast to the scenario proposed here for central Spain.

In Table 7 an unweighted and a weighted mean composition of the SCS xenolith suite is presented along with other estimates of global lower crust, together with peraluminous granulites interlayered with metagabbros of the Ivrea Zone (average stronalite). When compared with average lower crust in other areas and with model compositions (Wedepohl, 1995; McLennan & Taylor, 1996), the estimated composition of the lower crust in central Spain is clearly more felsic and richer in LILE and REE contents (Fig. 16). This agrees with recent estimations that result in a more felsic bulk composition of the lower crust, and suggests that the presence of a

Table 7: Mean major and trace element composition of Central Spain xenoliths and average lower-crustal estimates

	SCS xenolith suite		Lower-crustal estimates		Granulite terranes		Xenolith averages	
	Mean composition unweighted	Mean composition weighted*	Taylor & McLennan (1985)	Wedepohl (1995)	Whole deep crust of Calabria	Average stronalites Ivrea Zone	Massif Central	All xenoliths
SiO_2	58·00	61·53	54·4	58·0	55·4	61·1	56·3	50·5
TiO_2	1·13	1·02	0·9	0·84	1·6	1·21	1·1	1·0
Al_2O_3	19·59	17·11	16·1	15·7	17·8	17·8	17·1	16·5
Fe_2O_3(t)	9·26	8·19	11·8	8·10	12·0	9·67	8·80	10·0
MnO	0·09	0·10	0·2	0·12	0·19	0·14	0·11	0·15
MgO	3·45	3·47	6·3	5·3	5·6	3·4	5·0	7·8
CaO	1·36	1·55	8·5	6·8	2·4	2·5	5·5	9·7
Na_2O	2·10	2·53	2·8	2·9	2·0	1·6	2·1	2·4
K_2O	3·34	3·35	0·34	1·6	2·9	2·0	1·42	0·79
P_2O_5	0·16	0·16	—	0·2	0·08	0·10	0·16	0·23
Total	100·14	99·01	101·2	99·56	99·97	98·6	97·59	99·07
Ba	987	994	150	568	672	570	541	384
Rb	96	90	5·3	41	74	67	27	17
Sr	254	286	230	352	211	193	262	403
Ta	2·1	2·1	—	0·84		1·1		
Nb	17·3	15	6	11·3	17		11	11
Zr	200	206	70	165	213	285	174	84
Y	43	40	19	27·2	53	43		20
Th	7·15	5·74	1·1	6·6		14	5·8	1·6
U	0·47	0·47	0·3	0·93		1·2	0·6	0·4
Cr	219	178	235	228	102	156	222	308
Ni	66	65	135	99	74	60	62	137
Sc	17	17	36	25·3	63	25	25	34
V	155	139	285	149	224	170	167	214
Co	22	22	35	38	33	33	29	51
Cu	40	40	90	37·4		37	22	
Zn	90	83	—	79		109	87	
La	39·0	37·9	11	26·8		54	26	13
Ce	73·8	72·5	23	53·1		100	57	28
Nd	32·2	30·4	13	28·1		49		15
Sm	7·4	6·6	3·2	6·0		8·3	5·8	3·6
Eu	1·8	1·8	1·2	1·6		1·8	1·5	1·3
Gd	7·8	6·8	—	5·4		8·0		
Dy	7·5	6·7	—	4·7		7·8		
Yb	4·3	4·0	2·2	2·5		4·7	3·0	1·9
Lu	0·68	0·65	—	0·43		0·67		

*Weighted mean composition calculated from lithologic proportions (95% felsic + 5% pelitic) and mean compositions of xenolith types (Table 3).
References: Calabrian Massif (Maccarrone *et al.*, 1983), Ivrea Zone (Schnetger, 1994), Massif Central (Leyreloup *et al.*, 1977), average xenoliths (Rudnick, 1992).

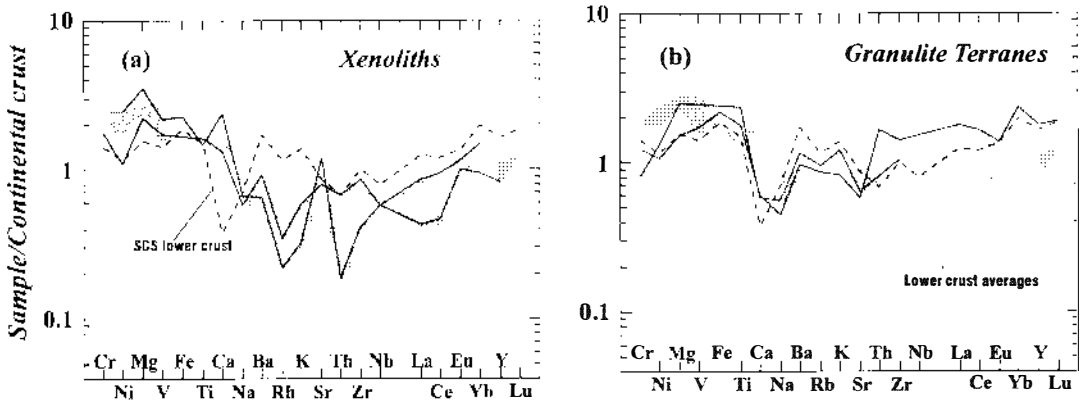

Fig. 16. Major and trace element diagrams normalized to average continental crust (Wedepohl, 1995) in which the mean weighted composition of SCS xenolith suite (dashed line) is compared with (a) other lower-crustal xenolith averages (continuous lines), lower crustal estimates (shaded field), and (b) granulite terranes (continuous lines) and lower-crustal estimates (shaded field) (data from Table 4). (See text for further explanation.)

mafic layer at the base of the continental crust is not a universal feature (Wedepohl, 1995; Le Pichon *et al.*, 1997). The felsic nature of the SCS lower crust is best shown in comparison with other lower-crustal xenolith suites which, on average, are more mafic than granulite terranes (Rudnick, 1992). The composition of the SCS lower crust resembles that of some peraluminous granulitic layers of exposed Hercynian granulite terranes (i.e. stronalites from Ivrea Zone, Fig. 16), which are also considered to be residues of high-pressure crustal melting from which granitic melt was extracted (Schnetger, 1994).

The essentially felsic character of the lower continental crust in this part of the Hercynian belt contrasts with the more mafic nature deduced for other European Hercynian areas (e.g. French Massif Central, Eifel, Ivrea, Calabria). The average lower continental crustal composition in central Spain, when compared with other estimates, is the most felsic lower crust yet known. This felsic character is not only shown by the granulitic xenolith suite but is also supported by geophysical data.

CONCLUSIONS

The study of the xenolith suite scavenged by early Mesozoic alkaline dykes in the Hercynian central region of central Spain reveals three main types of lower-crustal granulites. These are rare felsic to intermediate charnockites (<0·01% in volume), metapelitic (5% in volume) and common felsic meta-igneous types (95% in volume). *P–T* estimates in these granulites (850–950°C and 6–11 kbar) clearly indicate that these xenoliths come from the lower crust, although probably from different levels of this lower crust rather than from a single level.

Major and trace elements, and Sr–Nd isotopic compositions of the felsic and metapelitic types, are consistent with a restitic origin for these granulites after granitic melt extraction. Major and trace element modelling give reasonable values for the melting process comparable with experimental work and confirming that some of the Hercynian peraluminous granites could represent the average granitic liquid extracted. A mainly crustal origin for the peraluminous granites of the SCS is deduced. The isotopic shift of lower-crustal material toward bulk Earth composition substantially reduces the mantle contribution required by mixing models for granite petrogenesis.

ACKNOWLEDGEMENTS

Alfredo Fernández Larios and José González del Tánago from the CAI of Microscopía Electrónica (UCM) and Donald Herd from the University of St Andrews (UK) are thanked for their assistance with microprobe analyses. XRF and radiogenic isotope laboratories at Royal Holloway College (London) are University of London Intercollegiate Research facilities. Constructive comments and suggestions made by Calvin Miller, Heinz-G. Stosch, Pamela Kempton and an anonymous reviewer have greatly improved the quality of the manuscript. This work is included in the objectives of, and supported by, the PB96-0661 DGICYT project of the Ministerio de Educación y Cultura of Spain.

REFERENCES

Arth, J. G. (1976). Behaviour of trace elements during magmatic processes—a summary of theoretical models and their applications. *Journal of Research of the US Geological Survey* **4**, 41–47.

Banda, E., Suriñachs, E., Aparicio, A., Sterra, J. & Ruiz de la Parte, E. (1981). Crust and upper mantle structure of the Central Iberian Meseta (Spain). *Geophysical Journal of the Royal Astronomical Society* **67**, 779–789.

Barbero, L. (1995). Granulite facies metamorphism in the Anatectic Complex of Toledo (Spain): Late Hercynian tectonic evolution by crustal extension. *Journal of the Geological Society, London* **152**, 365–382.

Barbero, L., Villaseca, C., Rogers, G. & Brown, P. E. (1995). Geochemical and isotopic disequilibrium in crustal melting: an insight from the anatectic granitoids from Toledo, Spain. *Journal of Geophysical Research* **100**, 15745–15765.

Bea, F. (1996). Controls on the trace element composition of crustal melts. *Transactions of the Royal Society of Edinburgh: Earth Sciences* **87**, 33–41.

Bea, F. & Moreno-Ventas, I. (1985). Estudio petrológico de los granitoides del área centro-norte de la Sierra de Gredos (Batolito de Avila: Sistema Central Español). *Studia Geologica Salmanticensia* **20**, 137–174.

Beard, J. S., Abitz, R. J. & Lofgren, G. E. (1993). Experimental melting of crustal xenoliths from Kilbourne Hole, New Mexico, and implications for the contamination and genesis of magmas. *Contributions to Mineralogy and Petrology* **115**, 88–102.

Bernard-Griffiths, J., Peucat, J. J., Sheppard, S. & Vidal, P. (1985). Petrogenesis of Hercynian leucogranites from the southern Armorican Massif: contribution of REE and isotopic (Sr, Nd, Pb and O) geochemical data to the study of source rocks characteristics and age. *Earth and Planetary Science Letters* **74**, 235–250.

Bickle, M. J., Wickham, S. M., Chapman, H. J. & Taylor, H. P., Jr (1988). A strontium, neodymium and oxygen isotope study of hydrothermal metamorphism and crustal anatexis in the Trois Seigneurs Massif, Pyrenees, France. *Contributions to Mineralogy and Petrology* **100**, 399–417.

Bohlen, S. R. & Liotta, J. J. (1986). A barometer for garnet amphibolites and garnet granulites. *Journal of Petrology* **27**, 1025–1034.

Breiter, K. (1998). Geochemical evolution of P-rich granite suites: evidence from Bohemian massif. *Acta Universitatis Carolinae—Geologica* **42**, 7–19.

Brey, G. P., Nickel, K. G. & Kogarko, L. (1986). Garnet–pyroxene equilibria in the system $CaO–MgO–Al_2O_3–SiO_2$ (CMAS): prospects for simplified ('*T*-independent') lherzolite barometry and an eclogite-barometer. *Contributions to Mineralogy and Petrology* **92**, 448–455.

Carbó, A. & Capote, R. (1985). Estructura actual de la corteza en el Sistema Central Español e implicaciones geotectónicas. *Revista de la Real Academia de Ciencias Exactas, Físicas y Naturales* **79**, 625–634.

Carrington, D. P. & Harley, S. L. (1995). The stability of osumilite in metapelitic granulites. *Journal of Metamorphic Geology* **13**, 613–625.

Carrington, D. P. & Watt, G. R. (1995). A geochemical and experimental study of the role of K-feldspar during water-undersaturated melting of metapelites. *Chemical Geology* **122**, 59–76.

Cesare, B., Salvioli Mariani, E. & Venturelli, G. (1997). Crustal anatexis and melt extraction during deformation in the restitic xenoliths at El Hoyazo (SE Spain). *Mineralogical Magazine* **61**, 15–27.

Chappell, B. W., White, A. J. R. & Williams, I. S. (1991). *A Transverse Section through Granites of the Lachlan Fold Belt. Second Hutton Symposium, Excursion Guide. Record 1991/22*. Canberra, A.C.T.: Bureau of Mineral Resources.

Clarke, D. B., Halliday, A. N. & Hamilton, P. J. (1988). Neodymiun and strontium isotopic constraints on the origin of the peraluminous granitoids of the South Mountain Batholith, Nova Scotia. *Chemical Geology* **73**, 15–24.

Cocherie, A., Rossi, Ph., Fouillac, A. M. & Vidal, Ph. (1994). Crust to mantle contribution to granite genesis. An example from the Variscan batholith of Corsica, France, studied by trace element and Nd–Sr–O-isotope systematics. *Chemical Geology* **115**, 173–211.

Conrad, W. K., Nichols, I. A. & Wall, V. J. (1988). Water saturated and undersaturated melting of metaluminous and peraluminous crustal compositions at 1·0 GPa: evidence for the origin of silicic magmas in the Taupo Volcanic Zone, New Zealand, and other occurrences. *Journal of Petrology* **29**, 765–803.

Costa, S. & Rey, P. (1995). Lower crustal rejuvenation and growth during post-thickening collapse: insights from a crustal cross section through a Variscan metamorphic core complex. *Geology* **23**, 905–908.

Debon, F. & Le Fort, P. (1983). A chemical–mineralogical classification of common plutonic rocks and associations. *Transactions of the Royal Society of Edinburgh: Earth Sciences* **73**, 135–149.

de Bruiyn, H., van der Westuizen, W. A. & Schoch, A. E. (1983). The estimation of FeO, F and H_2O^+ by regression in microprobe analyses of natural biotites. *Journal of Trace and Microprobe Techniques* **1**, 399–413.

Downes, H. (1993). The nature of the lower continental crust of Europe: petrological and geochemical evidence from xenoliths. *Physics of the Earth and Planetary Interiors* **79**, 195–218.

Downes, H. & Duthou, J. L. (1988). Isotopic and trace element arguments for the lower-crustal origin of Hercynian granitoids and prehercynian orthogneisses, Massif Central (France). *Chemical Geology* **68**, 291–308.

Downes, H. & Leyreloup, A. (1986). Granulite xenoliths from the French Massif Central—petrology, Sr and Nd isotope systematics and model age estimates. In: Dawson, J. B., Carswell, D. A., Hall, J. & Wedepohl, K. H. (eds) *Nature of the Lower Continental Crust. Geological Society, London, Special Publication* **24**, 319–330.

Downes, H., Shaw, A., Williamson, B. J. & Thirlwall, M. F. (1997). Sr, Nd and Pb isotopic evidence for the lower crustal origin of Hercynian granodiorites and monzogranites, Massif Central, France. *Chemical Geology* **136**, 99–122.

Eberz, G. W., Clarke, D. B., Chatterjee, A. K. & Giles, P. S. (1991). Chemical and isotopic composition of the lower crust beneath the Meguma Lithotectonic Zone, Nova Scotia: evidence from granulite facies xenoliths. *Contributions to Mineralogy and Petrology* **109**, 69–88.

Ellis, D. J. (1980). Osumilite–sapphirine–quartz granulites from Enderby Land, Antarctica: *P–T* conditions of metamorphism, implications for garnet–cordierite equilibria and the evolution of the deep crust. *Contributions to Mineralogy and Petrology* **74**, 201–210.

England, P. C. & Thompson, A. B. (1986). Some thermal and tectonic models for crustal melting in continental collision zones. In: Coward, M. P. & Ries, A. (eds) *Collision Tectonics. Geological Society, London, Special Publication* **19**, 83–94.

Evensen, N. M., Hamilton, P. J. & O'Nions, R. K. (1978). Rare earth abundances in chondritic meteorites. *Geochimica et Cosmochimica Acta* **42**, 1199–1212.

Ferry, J. M. & Spear, F. S. (1978). Experimental calibration of the partitioning on Fe and Mg between biotite and garnet. *Contributions to Mineralogy and Petrology* **66**, 113–117.

Fuhrman, M. L. & Lindsley, D. H. (1988). Ternary-feldspar modeling and thermometry. *American Mineralogist* **73**, 201–215.

Ganguly, J. & Saxena, S. K. (1984). Mixing properties of aluminosilicate garnets: constraints from natural and experimental data, and applications to geothermo-barometry. *American Mineralogist* **69**, 88–97.

Gardien, V., Thompson, A. B., Grujic, D. & Ulmer, P. (1995). Experimental melting of biotite + plagioclase + quartz ± muscovite assemblages and implications for crustal melting. *Journal of Geophysical Research* **100**, 15581–15591.

Govindaraju, K. & Mévelle, G. (1987). Fully automated dissolution and separation methods for inductively coupled plasma atomic emission spectrometry rock analysis—application to the determination of rare-earth elements. *Journal of Analytical and Atomic Spectrometry* **2**, 615–621.

Grapes, R. H. (1985). Melting and thermal reconstitution of pelitic xenolith, Wehr volcano, East Eifel, West Germany. *Journal of Petrology* **27,** 343–396.

Gromet, L. P., Dymek, R. F., Haskin, L. A. & Korotev, R. L. (1984). The 'North American Shale Composite': its compilation, major and trace element characteristics. *Geochimica et Cosmochimica Acta* **48,** 2469–2482.

Hanchar, J. M., Miller, C. F., Wooden, J. L., Bennett, V. C. & Staude, J.-M. G. (1994). Evidence from xenoliths for a dynamic lower crust, Eastern Mojave Desert, California. *Journal of Petrology* **35,** 1377–1415.

Harley, S. L. (1984). An experimental study of partitioning of Fe and Mg between garnet and orthopyroxene. *Contributions to Mineralogy and Petrology* **86,** 359–373.

Hermann, J., Müntener, O., Trommsdorff, V., Hansmann, W. & Piccardo, G. B. (1997). Fossil crust-to-mantle transition, Val Malenco (Italian Alps). *Journal of Geophysical Research* **102**(B9), 20123–20132.

Hodges, K. V. & Spear, F. S. (1982). Geothermometry, geobarometry and the Al_2SiO_5 triple point at Mt. Moosilauke, New Hampshire. *American Mineralogist* **67,** 1118–1134.

Hoinkes, G. (1986). Effect of grossular-content in garnet on the partitioning of Fe and Mg between garnet and biotite. *Contributions to Mineralogy and Petrology* **92,** 393–399.

Holdaway, M. J. (1971). Stability of andalusite and the aluminium silicate phase diagram. *American Journal of Sciences* **271,** 97–131.

Holk, G. J. & Taylor, H. P., Jr (1997). $^{18}O/^{16}O$ homogenisation of the middle crust during anatexis: the Thor–Odin metamorphic core complex, British Columbia. *Geology* **25,** 31–34.

ILIHA DSS Group (1993). A deep seismic sounding investigation of lithospheric heterogeneity and anisotropy beneath the Iberian Peninsula. *Tectonophysics* **221,** 35–51.

Irving, A. J. & Frey, F. A. (1978). Distribution of trace element between garnet megacrysts and host volcanic liquids of kimberlitic to rhyolitic composition. *Geochimica et Cosmochimica Acta* **42,** 771–787.

Kern, H. (1990). Laboratory seismic measurements: an aid in the interpretation of seismic field data. *Terra Nova* **2,** 617–628.

Kretz, R. (1983). Symbols for rock-forming minerals. *American Mineralogist* **68,** 277–279.

Le Pichon, X., Henry, P. & Goffè, B. (1997). Uplift of Tibet: from eclogites to granulites—implications for the Andean Plateau and the Variscan belt. *Tectonophysics* **273,** 57–76.

Leyreloup, A., Dupuy, C. & Andriambololona, R. (1977). Catazonal xenoliths in French Neogene volcanic rocks: constitution of the lower crust. *Contributions to Mineralogy and Petrology* **62,** 283–300.

Loock, G., Stosh, H. G. & Seck, H. A. (1990). Granulite facies lower crustal xenoliths from the Eifel, West Germany: petrological and geochemical aspects. *Contributions to Mineralogy and Petrology* **105,** 25–41.

López Moro, F., López Plaza, M. & Martín Pozas, J. M. (1998). Characterization and origin of the alkali feldspar of granitoid rocks from the Variscan Anatectic Tormes Dome (West–Central Spain). *European Journal of Mineralogy* **10,** 535–550.

Maccarrone, E., Paglionico, A., Piccarreta, G. & Rottura, A. (1983). Granulite–amphibolite facies metasediments from the Serre (Calabria, Southern Italy): their protoliths and the processes controlling their chemistry. *Lithos* **16,** 95–111.

McCulloch, M. T. & Woodhead, J. D. (1993). Lead isotopic evidence for deep crustal-scale fluid transport during granite petrogenesis. *Geochimica et Cosmochimica Acta* **57,** 659–674.

McLennan, S. M. & Taylor, S. R. (1996). Heat flow and the chemical composition of continental crust. *Journal of Geology* **104,** 369–377.

MacRae, N. D. & Nesbitt, H. W. (1980). Partial melting of common metasedimentary rocks: a mass balance approach. *Contributions to Mineralogy and Petrology* **75,** 21–26.

Miller, C. F., Hanchar, J. M., Wooden, J. L., Bennett, V. C., Harrison, T. M., Wark, D. A. & Foster, D. A. (1992). Source region of a granite batholith: evidence from lower crustal xenoliths and inherited accessory minerals. *Transactions of the Royal Society of Edinburgh: Earth Sciences* **83,** 49–62.

Montel, J. M. & Vielzeuf, D. (1997). Partial melting of metagreywackes, Part II. Composition of minerals and melts. *Contributions to Mineralogy and Petrology* **128,** 176–196.

Moreno-Ventas, I., Rogers, G. & Castro, A. (1995). The role of hybridization in the genesis of Hercynian granitoids in the Gredos Massif, Spain: inferences from Sr–Nd isotopes. *Contributions to Mineralogy and Petrology* **120,** 137–149.

Nash, W. P. & Crecraft, H. R. (1985). Partition coefficients for trace elements in silicic magmas. *Geochimica et Cosmochimica Acta* **49,** 2309–2322.

Newton, R. C. & Perkins, D. I (1982). Thermodynamic calibration of geobarometers based on the assemblages garnet–plagioclase–orthopyroxene (clinopyroxene)–quartz. *American Mineralogist* **67,** 203–222.

Nichols, G. T., Berry, R. F. & Green, D. H. (1992). Internally consistent gahnitic spinel–cordierite–garnet equilibria in the FMASHZn system: geothermobarometry and applications. *Contributions to Mineralogy and Petrology* **111,** 362–377.

Nuez, J., Ubanell, A. G. & Villaseca, C. (1981). Diques lamprofíricos norteados con facies brechoidales eruptivas en la región de La Paramera de Ávila (Sistema Central Español). *Cuadernos do Laboratorio Xeoloxico de Laxe* **3,** 53–73.

Pankhurst, R. J. & Rapela, C. R. (1995). Production of Jurassic rhyolite by anatexis of the lower crust of Patagonia. *Earth and Planetary Science Letters* **134,** 25–36.

Patiño Douce, A. E. (1996). Effects of pressure and H_2O content on the compositions of primary crustal melts. *Transactions of the Royal Society of Edinburgh: Earth Sciences* **87,** 11–21.

Patiño Douce, A. E. & Beard, J. S. (1995). Dehydration-melting of biotite gneiss and quartz amphibolite from 3 to 15 kbar. *Journal of Petrology* **36,** 707–738.

Patiño Douce, A. E. & Johnston, A. D. (1991). Phase equilibria and melt productivity in the pelitic system: implications for the origin of peraluminous granitoids and aluminous granulites. *Contributions to Mineralogy and Petrology* **107,** 202–218.

Patiño Douce, A. E., Humphreys, D. E. & Johnston, A. D. (1990). Anatexis and metamorphism in tectonically thickened crust exemplified by the Sevier Hinterland, Western North America. *Earth and Planetary Science Letters* **97,** 290–315.

Paulssen, H. & Visser, J. (1993). The crustal structure in Iberia inferred from P-wave coda. *Tectonophysics* **221,** 111–123.

Peucat, J. J., Jegouzo, P., Vidal, P. & Bernard-Griffiths, J. (1988). Continental crust formation seen through the Sr and Nd isotope systematics of S-type granites in the Hercynian belt of western France. *Earth and Planetary Science Letters* **88,** 60–68.

Pin, C. (1989). Essai sur la chronologie et l'évolution géodynamique de la Chaîne Hercynienne d'Europe. Dr. Sci. Thesis, Université Blaise Pascal, Clermont-Ferrand, 470 pp.

Pin, C. (1990). Evolution of the lower crust in the Ivrea Zone: a model based on isotopic and geochemical data. In: Vielzeuf, D. & Vidal, Ph. (eds) *Granulites and Crustal Evolution*. Dordrecht: Kluwer Academic, pp. 87–110.

Pin, C. & Sills, J. D. (1986). Petrogenesis of layered gabbros and ultramafic rocks from Val Sesia, the Ivrea Zone, NW Italy: trace element and isotope geochemistry. In: Dawson, J. B., Carswell, D. A., Hall, J. & Wedepohl, K. H. (eds) *The Nature of the Lower Continental Crust. Geological Society, London, Special Publication* **24,** 231–249.

Pin, C., Binon, M., Belin, J. M., Barbarin, B. & Clemens, J. D. (1990). Origin of microgranular enclaves in granitoids: equivocal Sr–Nd evidence from Hercynian rocks in the Massif Central (France). *Journal of Geophysical Research* **95**(B11), 17821–17828.

Pinarelli, L. & Rottura, A. (1995). Sr and Nd isotopic study and Rb–Sr geochronology of the Béjar granites, Iberian Massif, Spain. *European Journal of Mineralogy* **7**, 577–589.

Qin, Z. (1991). Disequilibrium partial melting model and fractionation of highly incompatible trace elements during partial melting. *Geological Society of America, Abstracts with Programs* **23**, A45.

Reyes, J., Villaseca, C., Barbero, L., Quejido, A. & Santos, J. F. (1997). Desarrollo de un método de separación de Rb, Sr, Sm y Nd en rocas silicatadas para estudios isotópicos. *VII Congreso de Geoquímica de España* **1**, 46–55.

Rudnick, R. L. (1992). Xenoliths—samples of the lower continental crust. In: Fountain, D. M., Arculus, R. & Kay, R. W. (eds) *Continental Lower Crust*. Amsterdam: Elsevier, pp. 269–316.

Rudnick, R. L. & Presper, T. (1990). Geochemistry of intermediate- to high-pressure granulites. In: Vielzeuf, D. & Vidal, Ph. (eds) *Granulites and Crustal Evolution*. Dordrecht: Kluwer Academic, pp. 523–550.

Ruiz, J., Patchett, P. J. & Arculus, R. J. (1988). Nd–Sr isotopic composition of lower crustal xenoliths—evidence for the origin of mid-Tertiary felsic volcanics in Mexico. *Contributions to Mineralogy and Petrology* **99**, 36–43.

Rybach, L. & Muffler, L. J. P. (1981). *Geothermal Systems: Principles and Case Histories*. New York: John Wiley.

Sagredo, J. (1976). Enclaves granuliticos con hiperstena en los basaltos del NW de Cartagena (prov. Murcia). *Estudios Geológicos* **32**, 221–227.

Schermerhorn, L. J. G., Priem, H. N. A., Boelrijk, N. A. I., Hebeda, E. H., Verdumen, E. A. T. & Versclure, R. H. (1978). Age and origin of the Messejana dolerite fault dyke system (Portugal and Spain) in the light of the North Atlantic Ocean. *Journal of Geology* **86**, 229–309.

Schnetger, B. (1994). Partial melting during the evolution of the amphibolite-to-granulite-facies gneisses of the Ivrea Zone, northern Italy. *Chemical Geology* **113**, 71–101.

Sha, L. K. & Chappell, B. W. (1998). Contribution of feldspars to the whole-rock phosphorus budget of I- and S-type granites: a quantitative estimation. *Acta Universitatis Carolinae-Geologica* **42**, 125–128.

Singh, J. & Johannes, W. (1996). Dehydration melting of tonalites. Part II. Composition of melts and solids. *Contributions to Mineralogy and Petrology* **125**, 26–44.

Skjerlie, K. A. E. & Johnston, A. D. (1993). Fluid-absent melting behaviour of an F-rich tonalitic gneiss at mid-crustal pressures: implications for the generation of anorogenic granites. *Journal of Petrology* **34**, 785–815.

Stevens, G., Clemens, J. D. & Droop, G. T. R. (1997). Melt production during granulite-facies anatexis: experimental data from 'primitive' metasedimentary protoliths. *Contributions to Mineralogy and Petrology* **128**, 352–370.

Taylor, S. R. & McLennan, S. M. (1985). *The Continental Crust: its Composition and Evolution*. Oxford: Blackwell, 312 pp.

Ugidos, J. M., Valladares, M. I., Recio, C., Rogers, G., Fallick, A. E. & Stephens, W. E. (1997). Provenance of Upper Precambrian–Lower Cambrian shales in the Central Iberian Zone: evidence from a chemical and isotopic study. *Chemical Geology* **136**, 55–70.

Valverde Vaquero, P., Hernáiz, P. P., Escuder, J. & Dunning, G. R. (1995). Comparison of the pre-Cambrian and Palaeozoic evolution of the Sierra de Guadarrama (Central Iberian Zone, Spain) and the Gondwana margin, NFLD Appalachians (GMNA). *Terra Abstracts* **7**, 278.

Vialette, Y., Casquet, C., Fuster, J. M., Ibarrola, E., Navidad, M., Peinado, M. & Villaseca, C. (1987). Geochronological study of orthogneisses from the Sierra de Guadarrama (Spanish Central System). *Neues Jarbuch für Mineralogie, Monatshefte* **H10**, 465–479.

Vielzeuf, D. (1983). The spinel and quartz associations in high grade xenoliths from Tallante (S. E. Spain) and their potential use in geothermometry and barometry. *Contributions to Mineralogy and Petrology* **82**, 301–311.

Vielzeuf, D. (1984). Relations de phases dans le faciès granulite et implications géodynamiques. L'exemple des granulites des Pyrénées. Dr.Sci. Thesis, Université Blaise Pascal, Clermont-Ferrand, 288 pp.

Villaseca, C. & Nuez, J. (1986). Diques camptoníticos en el Sistema Central Español. *Estudios Geológicos* **42**, 69–77.

Villaseca, C., Huertas, M. J. & Nuez, J. (1992). Magmatismo post-orogénico y anorogénico en el Sistema Central Español. *Geogaceta* **11**, 34–38.

Villaseca, C., Barbero, L., Huertas, M. J., Andonaegui, P & Bellido, F. (1993). *A Cross-section through Hercynian Granites of Central Iberian Zone. Excursion Guide*. Madrid: Servicio de Publicaciones del CSIC.

Villaseca, C., Eugercios, L., Snelling, N., Huertas, M. J. & Castellón, T. (1995). Nuevos datos geocronológicos (Rb–Sr, K–Ar) de granitoides hercínicos de la Sierra de Guadarrama. *Revista de la Sociedad Geológica de España* **8**, 137–148.

Villaseca, C., Barbero, L. & Rogers, G. (1998). Crustal origin of Hercynian peraluminous granitic batholiths of central Spain: petrological, geochemical and isotopic (Sr, Nd) arguments. *Lithos* **43**, 55–79.

Voshage, H., Hofmann, A. W., Mazzuchelli, M., Rivalenti, G., Sinigoi, S., Raczeck, I. & Demarchi, G. (1990). Isotopic evidence from the Ivrea Zone for a hybrid lower crust formed by magmatic underplating. *Nature* **347**, 731–736.

Watt, G. R., Burns, I. M. & Graham, G. A. (1996). Chemical characteristics of migmatites: accessory phase distribution and evidence for fast melt segregation rates. *Contributions to Mineralogy and Petrology* **125**, 100–111.

Wedepohl, K. H. (1995). The composition of the continental crust. *Geochimica et Cosmochimica Acta* **59**, 1217–1232.

Wells, P. R. A. (1977). Pyroxene thermometry in simple and complex systems. *Contributions to Mineralogy and Petrology* **62**, 129–139.

Wickham, S. M. (1990). Isotopic modification of the continental crust: implications for the use of isotope tracers in granite petrogenesis. In: Asworth, J. R. & Brown, M. (eds) *High-temperature Metamorphism and Crustal Anatexis*. London: Unwin Hyman, pp. 124–148.

Wood, B. J. & Banno, S. (1973). Garnet–orthopyroxene and garnet–clinopyroxene relationships in simple and complex systems. *Contributions to Mineralogy and Petrology* **42**, 109–124.

APPENDIX A: GRANULITE SAMPLE DESCRIPTION

The 26 samples selected for study cover the spectrum of lower-crustal lithologies found as xenoliths in the SCS. These samples were also selected from a larger dataset of 74 xenoliths representing the best samples of greater size, less altered appearance and with no evidence of host lamprophyre infiltration. All the granulitic xenoliths are granoblastic in texture (Fig. A1) and many exhibit small-scale compositional banding marked by garnet (sillimanite)-rich bands sometimes alternating with quartz-rich layers (Fig. A1). Foliation is clearly defined by tabular pyroxene or sillimanite grains, but also by lamellar quartz (Fig. A1). Table A1 summarizes the petrographical and textural features of investigated samples.

Table A1. Granulite sample description

Sample	Locality	Texture	Major mineralogy
Charnockites			
U-3	La Paramera	equigr., foliated, fg	Pl, Qtz, Kfs, Opx
U-28	Bernuy-1	equigr., foliated, fg	Pl, Opx, Cpx
Felsic metaigneous			
U-140: 81845	Bernuy-1	equigr., massive, mg	Kfs, Pl, Grt, Opx
U-141: 81846	Bernuy-1	equigr., massive, mg	Pl, Kfs, Grt
U-49	La Paramera	equigr., banded, foliated, mg	Kfs, Qtz, Grt, Pl
U-50	La Paramera	inequigr., banded, cg	Grt, Kfs, Pl
U-92: 77747	La Paramera	equigr., banded, fg	Kfs, Qtz, Grt
U-93: 77748	La Paramera	equigr., massive, fg	Qtz, Kfs, Pl
U-137: 81841	Bernuy-2	inequigr., banded, mg	Qtz, Kfs, Pl, Grt, Phl
U-145: 95141	La Paramera	inequigr., banded, m–cg	Kfs, Qtz, Grt
U-146: 95142	La Paramera	inequigr., banded, mg	Kfs, Qtz, Grt, Pl
U-147: 95143	La Paramera	equigr., massive, mg	Qtz, Grt, Kfs, Pl
U-152: 95148	Peguerinos	inequigr., massive, m–cg	Kfs, Grt, Qtz
U-153: 95149	Peguerinos	equigr., banded, cg	Pl, Kfs, Qtz, Grt
U-155: 95151	Peguerinos	inequigr., banded, m–cg	Kfs, Qtz, Pl, Grt
U-156: 95152	Peguerinos	equigr., banded, mg	Kfs, Pl, Grt, Qtz
U-157: 95153	Peguerinos	inequigr., banded, cg	Pl, Qtz, Grt, Kfs
U-159: 99185	Peguerinos	inequigr., banded, foliated, cg	Qtz, Grt, Kfs, Pl
U-168:99193	Bernuy-2	inequigr., banded, m–cg	Kfs, Grt, Qtz, Pl
Pelitic			
U-10	La Paramera	inequigr., foliated, m–cg	Grt, Sil
U-42	La Paramera	equigr., banded, fg	Kfs, Grt, Qtz, Pl, Sil
U-46	La Paramera	equigr., massive, mg	Kfs, Grt, Qtz, Sil
U-90: 77745	La Paramera	inequigr., massive, m–cg	Grt, Pl, Kfs, Sil
U-91: 77746	La Paramera	inequigr., banded, m–cg	Kfs, Grt, Qtz, Pl, Sil
U-96: 77750	La Paramera	inequigr., banded, m–cg	Kfs, Grt, Qtz, Sil
AR-153: 81938	Peguerinos	equigr., foliated, fg	Grt, Sil, Kfs, Qtz

Abbreviations: fg, fine-grained; mg, medium-grained; cg, coarse-grained. Mineral abbreviations after Kretz (1983). Localities in universal grid coordinates: La Paramera diatreme outcrop (30TUK444842); Bernuy-1, quarry 1 km west from Bernuy Salinero village (30TUL645034); Bernuy-2, lamprophyre dyke 1 km northeast from Bernuy Salinero village (30TUL655038); Peguerinos, lamprophyre dyke rich in xenoliths 1 km west of Peguerinos village (30TUK951982). Samples of felsic ($n=4$) and pelitic ($n=1$) xenoliths from lamprophyre dykes of San Bartolomé de Pinares (located in Fig. 1) have not been selected for detailed analyses (mineral chemistry or whole-rock data).

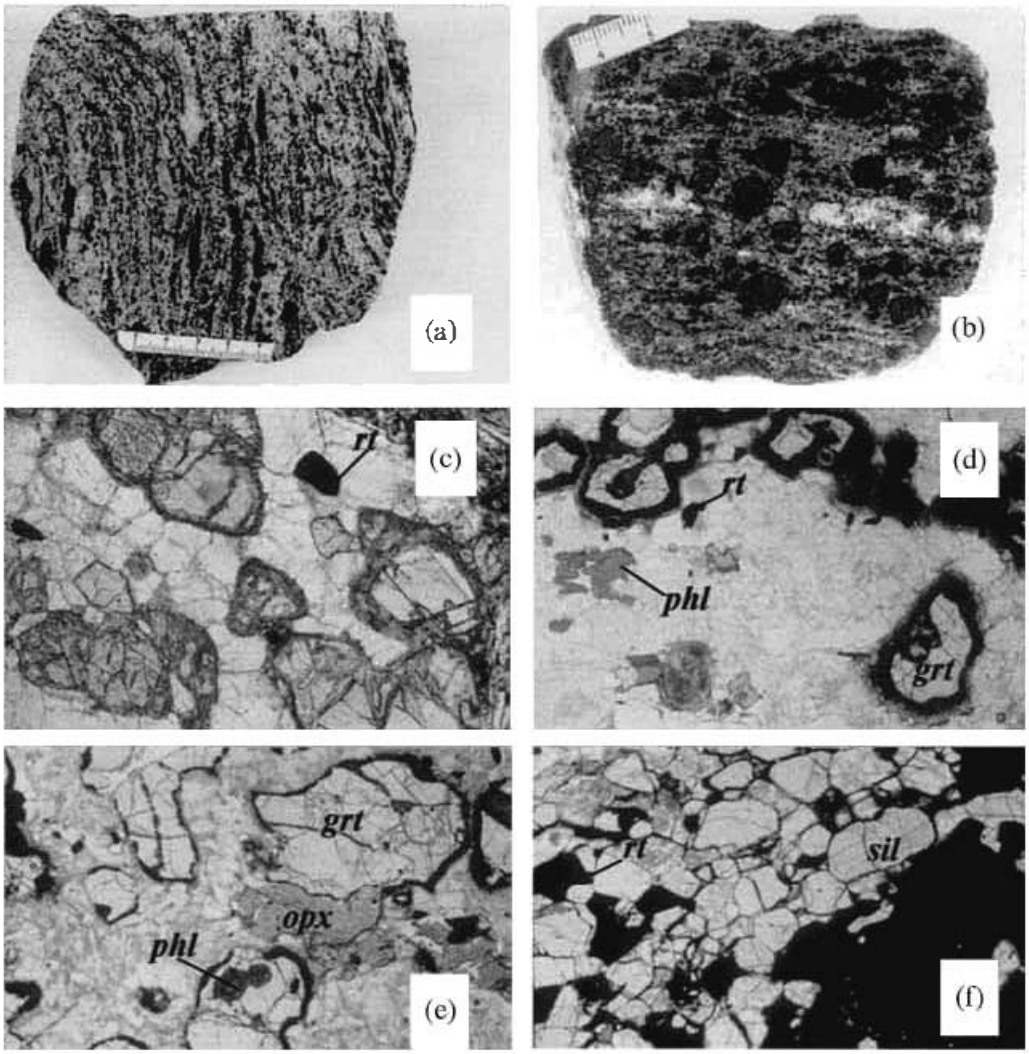

Fig. A1. Representative samples used in this study. Long dimension of hand samples is marked by scale in centimetres (a, b). Width of view of microphotographs is 4 mm (c–f). (a) Felsic metaigneous xenolith showing medium-grained equigranular banded structure; dark bands are composed of kelyphitic garnets. (b) Pelitic xenolith (sample 77750) showing coarser grain and more inequigranular banded structure. Dark crystals are coarse garnets. White band is a quartz-rich layer. (c) Charnockitic xenolith U-28 of granoblastic texture and showing sharp contact against the host dyke; rt, rutile. (d) Felsic metaigneous xenolith U-49. [Note the kelyphitic rims on garnet (grt) and the presence of phlogopite (phl) in the quartz–feldspathic matrix.] Dark rutile crystals (rt) are common. (e) Felsic metaigneous xenolith 81845 with orthopyroxene (opx) and garnet (grt). A small phlogopite crystal (phl) is included in garnet. (f) Pelitic xenolith U-90 showing most of the garnet transformed to kelyphitic aggregates. [Note the abundance of sillimanite crystals (sil) and subeuhedral dark rutile crystals (rt).]

APPENDIX B: PARTITION COEFFICIENTS USED IN THE TRACE ELEMENT MODELLING

K_d values for LILE from Arth (1976) except Rb for K-feldspar, which is taken from Schnetger (1994). Y for plagioclase and garnet from Arth (1976), for K-feldspar and biotite from Schnetger (1994) and for monazite is extrapolated between K_d values for Dy and Yb. REE for plagioclase and K-feldspar are taken from Nash & Crecraft (1985), REE for biotite from Arth (1976), REE for garnet from Irving & Frey (1978) and REE for monazite from Cocherie *et al.* (1994).

Table B1. Partition coefficients (K_d)

	Plg	Kfs	Garnet	Biotite	Monazite
Ba	0·36	6·12	0·017	6·36	
Rb	0·048	0·90	0·009	3·26	
Sr	2·84	3·87	0·015	0·12	
Y	0·10	0·005	35·00	1·40	450
La	0·38	0·08	0·39	0·05	5260
Ce	0·267	0·037	0·69	0·037	5060
Nd	0.203	0·035	0·603	0·044	4500
Sm	0·165	0·025	2·035	0·058	3830
Eu	5·417	4·45	0·515	0·145	482
Gd	0·125	0·025	6·975	0·082	1750
Dy	0·112	0·055	28·6	0·097	900
Yb	0·09	0·03	43·47	0·179	173
Lu	0·092	0·033	39·775	0·185	115